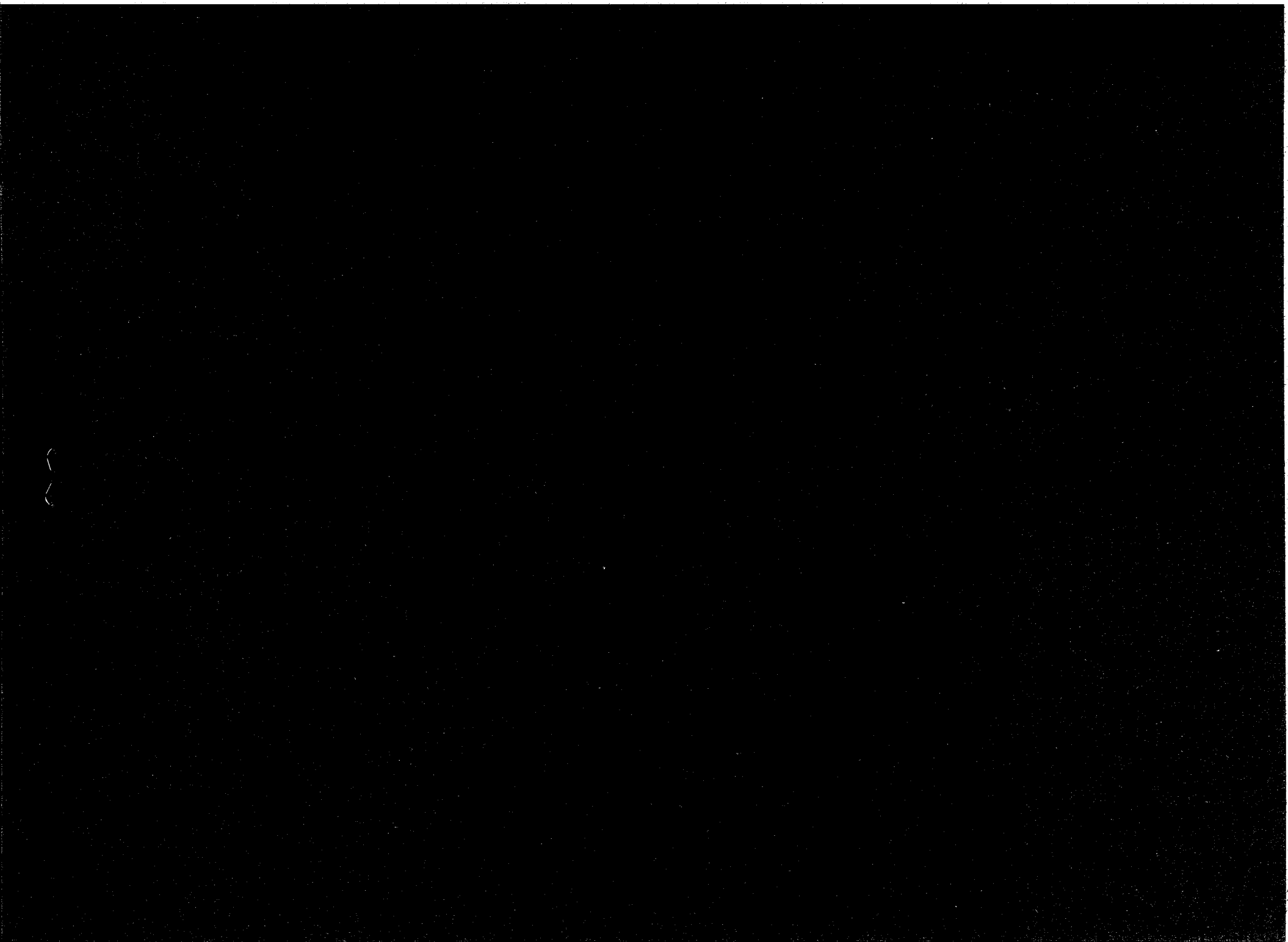

NASA Technical Memorandum 4237

Static Internal Performance of an Axisymmetric Nozzle With Multiaxis Thrust-Vectoring Capability

George T. Carson, Jr., and Francis J. Capone
Langley Research Center
Hampton, Virginia

National Aeronautics and
Space Administration
Office of Management
Scientific and Technical
Information Division

1991

Summary

An investigation has been conducted in the static test facility of the Langley 16-Foot Transonic Tunnel to determine the internal performance characteristics of a multiaxis thrust-vectoring axisymmetric nozzle. Thrust vectoring for this nozzle was achieved by deflection of only the divergent section of the nozzle. The effects of nozzle power setting and divergent flap length were studied at nozzle deflection angles of 0° to 30° at nozzle pressure ratios up to 8.0.

The results of this investigation indicated that vectoring of the exhaust flow was achieved with essentially no turning losses. Resultant pitch vector angles greater than the geometric pitch vector angle occurred at nozzle pressure ratios for which flow separation was not present in the nozzle. The nozzle with the longer divergent flaps had higher resultant thrust performance during vectored operation and had higher turning angles at afterburner power settings.

Introduction

The mission requirements for the next generation of aircraft may dictate a highly versatile vehicle capable of supersonic cruise, short takeoffs and landings, and maneuverability at high angles of attack. Several studies have shown that significant advantages in air combat are gained with the ability to perform transient maneuvers at high angles of attack, including brief excursions into post-stall conditions (refs. 1 to 3). However, the angle-of-attack envelope of advanced fighters can be limited because of degraded stability characteristics and inadequate aerodynamic control power at high angles of attack. Providing controls that maintain high levels of effectiveness will allow future fighters to exploit a much-expanded angle-of-attack envelope.

One promising method to provide large control moments not dependent upon angle of attack is vectoring the exhaust flow. A number of investigations, conducted both at static conditions (wind off) and at forward speeds, have verified the capability of multifunction nozzles to provide pitch and yaw thrust vectoring (refs. 4 to 8). In general, most of these studies have been concerned with nonaxisymmetric nozzles. Multiaxis thrust vectoring capability for axisymmetric nozzles has been achieved through the use of post-exit vanes (ref. 9) or a gimballed device (ref. 10). However, large weight penalties can occur with the use of both post-exit vanes and gimballed devices. An alternate nozzle design, in which thrust vectoring is achieved by deflection of the divergent section of the nozzle, has been tested. This concept permits divergent flap vectoring through the use of synchronizing rings and actuators and by universal joint attachments at the throat.

The purpose of this investigation was to determine the internal performance characteristics of this multiaxis thrust-vectoring axisymmetric nozzle. Fixed-geometry nozzles, representing both dry and maximum afterburning power settings, were tested with two divergent flap lengths. Internal static pressures were also measured. This investigation was conducted in the static test facility of the Langley 16-Foot Transonic Tunnel.

Symbols

All forces and moments (with the exception of resultant gross thrust) are referred to the model centerline (body axis). The model (balance) moment reference center was located at station 29.39. A discussion of the data reduction procedure and definitions of the force and moment terms and the propulsion relationships used herein can be found in reference 11.

A/B	afterburning
A_e	nozzle exit area, in^2
A_t	nozzle throat area, in^2
d_e	nozzle exit diameter, in
d_t	nozzle throat diameter, in
F	measured thrust along body axis, lbf
F_i	ideal isentropic gross thrust $w_p \left\{ \frac{RT_{t,j}}{g^2} \frac{2\gamma}{\gamma-1} \left[1 - \left(\frac{1}{\mathrm{NPR}} \right)^{(\gamma-1)/\gamma} \right] \right\}^{1/2}$, lbf
F_N	measured normal force, lbf
F_r	resultant gross thrust, $\sqrt{F^2 + F_N^2 + F_Y^2}$, lbf
F_Y	measured side force, lbf
g	gravitational constant, 32.174 ft/sec
L_f	divergent flap length, in.
l	reference length, 1.00 in.
NPR	nozzle pressure ratio, $p_{t,j}/p_a$
$(\mathrm{NPR})_{\mathrm{des}}$	design pressure ratio for ideally expanded flow
PM	measured pitching moment, in-lb
p	local static pressure, psi
p_a	ambient pressure, psi
$p_{t,j}$	jet total pressure, psi
R	gas constant for air, 1716 ft^2/sec^2-°R

Sta.	model station, in.
$T_{t,j}$	jet total temperature, °R
w_i	ideal weight-flow rate, lbf/sec
w_p	measured weight-flow rate, lbf/sec
x	longitudinal distance measured from nozzle throat, in.
YM	measured yawing moment, in-lb
γ	ratio of specific heats for air, 1.4
δ_p	resultant pitch vector angle, $\tan^{-1}\frac{F_N}{F}$, deg
$\delta_{v,p}$	geometric pitch vector angle measured from nozzle centerline, positive for downward deflection, deg
$\delta_{v,y}$	geometric yaw vector angle measured from nozzle centerline, positive deflection to left looking upstream, deg
δ_y	resultant yaw vector angle, $\tan^{-1}\frac{F_Y}{F}$, deg
ϕ	meridian angle, measured from top of nozzle, positive counterclockwise looking upstream, deg

Apparatus and Procedure

Static Test Facility

This investigation was conducted in the static test facility of the Langley 16-Foot Transonic Tunnel. The test apparatus is installed in a room with a high ceiling. The jet exhausts to atmosphere through a ceiling vent aft of the nozzle test apparatus. The control room is remotely located from the test area, and a closed-circuit television camera is used to observe the model. This facility uses the same clean, dry air supply as the 16-Foot Transonic Tunnel and uses a similar air-control system—including valving, filters, and a heat exchanger (to operate the jet flow at constant stagnation temperature).

Single-Engine Propulsion Simulation System

A sketch of the single-engine air-powered simulation system is presented in figure 1(a) with a typical nozzle configuration installed; a photograph of the test apparatus is shown in figure 1(b).

An external high-pressure air system provided a continuous flow of clean, dry air at a controlled temperature of about 540°R at the nozzles. This high-pressure air was varied up to approximately 8 atm (1 atm = 14.696 psi) and was brought through the dolly-mounted support strut by six tubes that connect to a high-pressure plenum chamber. As shown in figure 2, the air was then discharged perpendicularly into the model low-pressure plenum through eight multiholed sonic nozzles equally spaced around the high-pressure plenum. This method was designed to minimize any forces imposed by the transfer of axial momentum as the air passed from the nonmetric high-pressure plenum to the metric (mounted on the force balance) low-pressure plenum. Two flexible metal bellows were used as seals and served to compensate for axial forces caused by pressurization. The air was then passed from the model low-pressure plenum through a choke plate, instrumentation section, adapter section, and test nozzle as shown in figure 1(a).

Nozzle Design and Model

The nozzle design concept depicted in figure 3 permits pitch and yaw vectoring of the axisymmetric nozzle through deflection of the divergent section of the nozzle. This is accomplished through the use of synchronizing rings and actuators, universal joint attachments at the nozzle throat, and a circumferentially segmented divergent nozzle flap.

The subscale models of the axisymmetric nozzle tested during this investigation are shown in figures 4 and 5. These nozzles are fixed-geometry representations of a variable-geometry nozzle at a dry (or cruise) power setting and at an afterburning power setting. The nozzle expansion ratio was 1.35 for both power settings, and the design pressure ratio was 5.01. Two divergent flap lengths were tested for each nozzle power setting. Use of the shorter flap could result in lower nozzle weight. Geometric pitch vector angles of 0°, 10°, 20°, and 30° were provided and are shown in figure 5. Photographs of the dry power nozzle with the short flap are shown in figure 6. Some limited combined pitch/yaw thrust-vectoring configurations were tested by rotating a particular nozzle 45° at the adapter/nozzle connection.

Instrumentation

A six-component strain-gauge balance was used to measure forces and moments on the model (figs. 1(a) and 2). Flow conditions in the nozzle were determined from eight total-pressure probes and two total-temperature probes at Sta. 37.65 in the instrumentation section aft of the choke plate (Sta. 34.11). Nozzle total pressure and temperature are determined from the average of these measurements. Weight flow of the high-pressure air supplied to the exhaust nozzle was measured by a pair of critical-flow venturis. Internal static pressure orifices

were located along the divergent section of the nozzle as shown in figure 7. All pressures were measured with individual pressure transducers.

Data Reduction

All data were recorded simultaneously on magnetic tape. Approximately 50 frames of data, taken at a rate of 10 frames per second, were used for each data point; average values were used in computations. Data were obtained in an ascending order of $p_{t,j}$.

The basic performance parameters used for the presentation of results were $F/F_i, F_N/F_i, F_Y/F_i$, $F_r/F_i, \delta_p, \delta_y$, and w_p/w_i. With the exception of resultant gross thrust F_r, all force data in this report are referenced to the body axis (centerline). The component internal thrust ratios, $F/F_i, F_N/F_i$, and F_Y/F_i, represent the ratio of actual nozzle thrust (along the body axis, vertical axis, and lateral axis, respectively) to ideal nozzle thrust, where ideal nozzle thrust is based on measured weight-flow rate and total pressure and temperature conditions in the instrumentation section, as defined by the equations in the symbols definitions.

The balance force measurements from which actual thrust is subsequently obtained are initially corrected for model weight tares and balance interactions. Although the bellows arrangement was designed to eliminate pressure and momentum interactions with the balance, small bellows tares on all balance components still exist. These tares result from a small pressure difference between the ends of the bellows when internal velocities are high and from small differences in the forward and aft bellows spring constants when the bellows are pressurized. As discussed in reference 4, these bellows tares were determined by testing calibration nozzles with known performance over a range of expected normal- and side-force and yawing-, pitching-, and rolling-moment loadings. The balance data were then corrected in a manner similar to that discussed in references 4 and 11. The resultant gross thrust F_r used in the resultant thrust ratio F_r/F_i was then determined from these corrected balance data, as were the individual component force ratios, F/F_i, F_N/F_i, and F_Y/F_i. Significant differences between F_r/F_i and F/F_i occur when exhaust flow is directed away from the axial direction. The individual force ratios are presented to allow a direct comparison of normal- and side-force magnitudes relative to axial-force values. In addition, normalized moment ratios $\mathrm{PM}/F_i l$ and $\mathrm{YM}/F_i l$ are also presented. Resultant thrust vector angles in the longitudinal (pitch) plane δ_p and the lateral (yaw) plane δ_y are presented for evaluating the exhaust-flow turning capability of the various thrust-vectored configurations.

The nozzle discharge coefficient w_p/w_i is the ratio of measured weight flow to ideal weight flow, where ideal weight flow is based on jet total pressure $p_{t,j}$, jet total temperature $T_{t,j}$, and measured nozzle throat area. The nozzle discharge coefficient reflects the ability of a nozzle to pass weight flow and is reduced by any momentum and vena contracta losses (effective throat area less than measured throat area A_t).

Presentation of Results

The results of this investigation are presented in both tabular and plotted form. Table 1 is an index to the tabular results contained in tables 2 to 21. Static performance data are presented in tables 2 to 5 and nozzle internal pressure ratios are given in tables 6 to 21. Internal pressure distributions for selected configurations are presented in figures 8 to 11 and static performance characteristics for the nozzles are given in figures 12 to 19 as follows:

Discussion

Internal Pressure Distributions

Internal static pressure distributions are presented in figures 8 to 11 for the dry and A/B power

nozzles with the short divergent flap section at pitch vector angles of 0° and 20°. These pressure distributions are typical of the flow characteristics of the other nozzles tested (pressure data contained in tables). The static pressure distributions on the divergent flap section of the unvectored nozzles at NPR > 2.5 show a sudden pressure rise across an exhaust-flow shock, which is indicative of shock-induced separation from the wall. This occurred for both the dry power nozzle (fig. 8(a)) and the A/B power nozzle (fig. 10(a)). Similar results were obtained for these two nozzles with the long divergent flap sections.

When vectored, the nozzles have significantly different flow characteristics than the unvectored nozzles. As shown in figure 8(b), pressures along the top ($\phi = 0°$) of the nozzle were much greater than those for the unvectored nozzle. Along the bottom ($\phi = 180°$) of the dry power nozzle with the short divergent flap, the flow was completely separated, up to a pressure ratio of 3.50. Figure 9 indicates that this flow separation extended at least 45° around from the bottom of the nozzle. For the dry power nozzle with the long flaps, which had a smaller divergent flap expansion angle, these conditions were evident only up to NPR = 2.0. The A/B power nozzle exhibited similar flow characteristics (figs. 10 and 11).

The pressure distributions also indicate that the actual nozzle throat for the vectored nozzles is highly inclined. For $\delta_{v,p} = 0°$, the actual throat probably coincided with the geometric throat and could have been better defined with additional pressure measurements made nearer the throat. However, for $\delta_{v,p} = 20°$, the actual throat ($p/p_{t,j} = 0.528$) occurs at $x/L_f \approx 0.7$ along the top of the nozzle and at $x/L_f \approx 0.1$ along the bottom at NPR = 2.0 (fig. 8(b) or 10(b)). At NPR > 3.50, the throat has moved forward along the top to $x/L_f \approx 0.5$. Because of this highly inclined throat, turning of the flow is accomplished at essentially subsonic conditions, which in turn will result in little or no turning losses. Large thrust losses will result with supersonic flow turning, which occurs, for example, with post-exit vanes used for thrust vectoring (ref. 9).

Nozzle Static Performance

Static performance characteristics for the various nozzles showing the effects of pitch and yaw thrust vectoring are shown in figures 12 to 17. Static nozzle performance is presented as internal thrust ratio F/F_i, resultant thrust ratio F_r/F_i, resultant pitch vector angle δ_p, resultant yaw vector angle δ_y, and nozzle discharge coefficient w_p/w_i. Peak nozzle performance for the dry power unvectored nozzles generally occurred between nozzle pressure ratios of 5.0 to 6.0. Typically, the peak nozzle performance is obtained at the jet nozzle pressure ratio required for fully expanded flow (the design pressure ratio), which for the current nozzles was 5.01 (figs. 12(a) and 14(a)). Peak nozzle performance was not obtained for the A/B power nozzles because facility airflow capacity restricted the maximum obtainable pressure ratio.

A comparison between the unvectored and vectored nozzles shows that differences in peak or maximum obtainable nozzle performance were less than 1 percent of the internal resultant gross thrust ratio, indicating little or no losses due to flow turning. This is because the flow was turned essentially at subsonic Mach numbers as previously discussed. (See, for example, fig. 12(a) or 17(a).) All the nozzles were effective in vectoring the thrust when the nozzle pressure ratio was large enough to reduce the amount of flow separation on the bottom of the nozzle. When extensive flow separation was not present on the lower divergent flaps, thrust vector angles equal to or greater than the geometric angles were obtained. For example, this occurs for the dry power nozzle with the short flap at NPR = 4.0 (fig. 12(a)), the lowest pressure ratio for which extensive flow separation was not present (fig. 8(b)). Similarly, figure 17(a) shows that maximum pitch vector angles were achieved at NPR = 3.0 for the A/B power nozzle with the long flap, which also was the NPR for attached flow on the bottom of the nozzle. These results are similar to those obtained for two-dimensional convergent-divergent nozzles (refs. 4 and 5).

The maximum measured vector angle for each of the nozzles was generally reached below the design pressure ratio and decreased as pressure ratio was increased. This effect of thrust angularity varying with nozzle pressure ratio is common in nonaxisymmetric nozzles whenever one flap is longer than the other relative to the exhaust flow centerline (exit plane perpendicular to centerline). A similar situation exists for the axisymmetric nozzles of the present investigation, where the bottom portion of the divergent flap section extends beyond that of the top (fig. 5). This type of nozzle geometry presents expansion surfaces of unequal length for the flow to work against, such that one side of the exhaust flow is contained longer by the divergent flap while the other side of the exhaust flow is unbounded. When either the dry or the A/B power nozzles were both pitch and yaw vectored, nearly equal resultant pitch and yaw vector angles were obtained (figs. 13(a) and 16(a)).

A comparison of internal performance for the dry and A/B power nozzles with the short and long divergent flaps is made in figures 18 and 19, respectively. Figure 18 shows that the dry power nozzles with these two flap lengths had essentially the same

resultant thrust ratios for $\delta_{v,p} = 0°$ and 10°. At $\delta_{v,p} = 20°$ and 30°, the nozzle with the long flaps had higher thrust performance at NPR > 3.0, which probably resulted from lower divergence losses for these nozzles at the higher nozzle pressure ratios. The longer flap nozzle had higher resultant pitch vector angles at NPR = 2.5 to 4.0 (depending on vectored nozzle), which were the pressure ratios at which the nozzle with the shorter flap still exhibited flow separation. Similar results were obtained for the A/B power nozzle (fig. 19) except that the resultant pitch vector angles were greater for the nozzle with longer flaps over the NPR range tested.

Concluding Remarks

An investigation has been conducted at static conditions in order to determine the internal performance characteristics of a multiaxis thrust-vectoring axisymmetric nozzle. Thrust vectoring for this nozzle would be achieved by deflection of only the divergent section of the nozzle. The effects of nozzle power setting and divergent flap length were studied at nozzle deflection angles of 0° and 30°. This investigation was conducted in the static test facility of the Langley 16-Foot Transonic Tunnel at nozzle pressure ratios up to 8.0.

The results of this investigation indicated that vectoring of the exhaust flow was achieved with essentially no turning losses. Resultant pitch vector angles greater than the geometric pitch vector angle occurred at nozzle pressure ratios for which flow separation was not present in the nozzle. The nozzles with the longer flaps had higher resultant thrust performance during vectored operation and higher turning angles at afterburning power settings.

NASA Langley Research Center
Hampton, VA 23665-5225
November 30, 1990

References

1. Herbst, W. B.: Future Fighter Technologies. *J. Aircr.*, vol. 17, no. 8, Aug. 1980, pp. 561–566.
2. Costes, Philippe: Investigation of Thrust Vectoring and Post-Stall Capability in Air Combat. *A Collection of Technical Papers, Part 2—AIAA Guidance, Navigation and Control Conference, Aug. 1988,* pp. 893–905. (Available as AIAA-88-4160-CP.)
3. Powers, Sidney A.; and Schellenger, Harvey G.: The X-31: High Performance at Low Cost. AIAA-89-2122, July–Aug. 1989.
4. Capone, Francis J.: *Static Performance of Five Twin-Engine Nonaxisymmetric Nozzles With Vectoring and Reversing Capability.* NASA TP-1224, 1978.
5. Capone, Francis J.; and Mason, Mary L.: *Multiaxis Aircraft Control Power From Thrust Vectoring at High Angles of Attack.* NASA TM-87741, 1986.
6. Leavitt, Laurence D.: Summary of Nonaxisymmetric Nozzle Internal Performance From the NASA Langley Static Test Facility. AIAA-85-1347, July 1985.
7. Capone, Francis J.; and Bare, E. Ann: *Multiaxis Control Power From Thrust Vectoring for a Supersonic Fighter Aircraft Model at Mach 0.20 to 2.47.* NASA TP-2712, 1987.
8. Berrier, Bobby L.: *Results From NASA Langley Experimental Studies of Multiaxis Thrust Vectoring Nozzles.* SAE Tech. Paper Ser. 881481, Oct. 1988.
9. Berrier, Bobby L.; and Mason, Mary L.: *Static Performance of an Axisymmetric Nozzle With Post-Exit Vanes for Multiaxis Thrust Vectoring.* NASA TP-2800, 1988.
10. Mace, J.; Smereczniak, P.; Krekeler, G.; Bowers, D.; MacLean, M.; and Thayer, E.: Advanced Thrust Vectoring Nozzles for Supercruise Fighter Aircraft. AIAA-89-2816, July 1989.
11. Mercer, Charles E.; Berrier, Bobby L.; Capone, Francis J.; Grayston, Alan M.; and Sherman, C. D.: *Computations for the 16-Foot Transonic Tunnel—NASA, Langley Research Center, Revision 1.* NASA TM-86319, 1987. (Supersedes NASA TM-86319, 1984.)

Table 1. Index to Data in Tables 2 to 21

Power setting	L_f/d_t	$\delta_{v,p}$, deg	$\delta_{v,y}$, deg	Performance data tables	Pressure data tables
Dry	0.88	0	0	2	6
		10	0	2	7
		20	0	2	8
		30	0	2	9
		14.14	14.14	2	
Dry	1.32	0	0	3	10
		10	0	3	11
		20	0	3	12
		30	0	3	13
A/B	0.64	0	0	4	14
		10	0	4	15
		20	0	4	16
		30	0	4	17
		7.07	7.07	4	
		14.14	14.14	4	
A/B	0.97	0	0	5	18
		10	0	5	19
		20	0	5	20
		30	0	5	21

Table 2. Static Characteristics for Dry Power Nozzle With Short Flap

(a) $\delta_{v,p} = 0°, \delta_{v,y} = 0°$

NPR	w_p/w_i	F_r/F_i	F/F_i	δ_p	δ_y	F_N/F_i	PM/$F_i l$	F_Y/F_i	YM/$F_i l$
1.51	0.9831	0.8814	0.8813	-0.71	0.04	-0.0110	0.0031	0.0006	0.0113
2.01	0.9486	0.9014	0.9014	-0.31	-0.17	-0.0049	0.0166	-0.0026	0.0088
2.51	0.9445	0.9285	0.9285	-0.01	-0.09	-0.0002	0.0119	-0.0014	0.0001
3.01	0.9447	0.9521	0.9521	0.07	0.00	0.0011	0.0078	-0.0001	-0.0075
3.51	0.9453	0.9675	0.9675	0.12	-0.04	0.0021	0.0050	-0.0006	-0.0050
4.01	0.9445	0.9767	0.9767	0.13	-0.02	0.0022	0.0054	-0.0003	-0.0076
5.00	0.9440	0.9843	0.9843	0.15	-0.02	0.0026	0.0024	-0.0004	-0.0081
6.02	0.9438	0.9858	0.9858	0.12	0.00	0.0021	-0.0021	0.0001	-0.0065
7.00	0.9434	0.9854	0.9854	0.11	0.03	0.0019	-0.0035	0.0005	-0.0078
7.81	0.9433	0.9851	0.9851	0.11	0.04	0.0018	-0.0051	0.0008	-0.0068

(b) $\delta_{v,p} = 10°, \delta_{v,y} = 0°$

NPR	w_p/w_i	F_r/F_i	F/F_i	δ_p	δ_y	F_N/F_i	PM/$F_i l$	F_Y/F_i	YM/$F_i l$
1.50	0.9326	0.9270	0.9254	3.30	-0.29	0.0533	-0.5840	-0.0047	0.0234
1.99	0.9408	0.9543	0.9536	2.08	-0.07	0.0347	-0.3335	-0.0012	0.0075
2.50	0.9460	0.9487	0.9443	5.50	-0.42	0.0909	-0.6726	-0.0070	0.0450
3.01	0.9485	0.9547	0.9341	11.93	-0.26	0.1973	-1.3962	-0.0042	0.0270
3.51	0.9471	0.9681	0.9408	13.64	-0.14	0.2282	-1.6112	-0.0022	0.0163
4.01	0.9461	0.9758	0.9469	13.98	-0.10	0.2357	-1.6521	-0.0016	0.0135
5.00	0.9460	0.9825	0.9553	13.51	-0.04	0.2295	-1.5835	-0.0006	0.0109
6.00	0.9458	0.9839	0.9583	13.11	-0.02	0.2232	-1.5203	-0.0003	0.0091
7.00	0.9458	0.9834	0.9586	12.89	-0.05	0.2193	-1.4707	-0.0009	0.0109
8.00	0.9453	0.9822	0.9580	12.75	-0.06	0.2167	-1.4328	-0.0010	0.0073

(c) $\delta_{v,p} = 20°, \delta_{v,y} = 0°$

NPR	w_p/w_i	F_r/F_i	F/F_i	δ_p	δ_y	F_N/F_i	PM/$F_i l$	F_Y/F_i	YM/$F_i l$
1.50	0.8525	0.9500	0.9315	11.30	-0.32	0.1862	-1.4268	-0.0051	0.0091
2.00	0.8914	0.9623	0.9388	12.69	-0.29	0.2114	-1.4999	-0.0047	0.0153
2.50	0.9136	0.9647	0.9295	15.52	-0.25	0.2581	-1.7926	-0.0041	0.0179
3.00	0.9190	0.9680	0.9206	18.00	-0.04	0.2992	-2.0478	-0.0006	-0.0025
3.50	0.9200	0.9712	0.9087	20.68	-0.17	0.3430	-2.3351	-0.0026	0.0132
4.01	0.9194	0.9749	0.8876	24.44	-0.08	0.4033	-2.7350	-0.0012	0.0128
5.02	0.9196	0.9811	0.9000	23.46	-0.12	0.3905	-2.6089	-0.0019	0.0103
6.02	0.9191	0.9824	0.9063	22.70	-0.08	0.3791	-2.5043	-0.0013	0.0086
7.01	0.9194	0.9819	0.9087	22.26	-0.12	0.3720	-2.4270	-0.0019	0.0108
8.00	0.9182	0.9814	0.9107	21.88	-0.12	0.3657	-2.3679	-0.0020	0.0074

Table 2. Concluded

(d) $\delta_{v,p} = 30°, \delta_{v,y} = 0°$

NPR	w_p/w_i	F_r/F_i	F/F_i	δ_p	δ_y	F_N/F_i	PM/$F_i l$	F_Y/F_i	YM/$F_i l$
1.51	0.7715	0.9402	0.8785	20.86	-0.16	0.3348	-2.3603	-0.0025	0.0422
2.00	0.8260	0.9486	0.8672	23.90	-0.36	0.3843	-2.6117	-0.0054	0.0278
2.50	0.8531	0.9555	0.8607	25.74	-0.10	0.4149	-2.7885	-0.0016	0.0146
3.01	0.8597	0.9614	0.8532	27.45	-0.20	0.4432	-2.9628	-0.0030	0.0225
3.50	0.8571	0.9644	0.8401	29.42	-0.37	0.4737	-3.1576	-0.0054	0.0421
4.00	0.8572	0.9696	0.8311	31.01	-0.42	0.4995	-3.3087	-0.0062	0.0445
5.00	0.8567	0.9755	0.8339	31.26	-0.32	0.5063	-3.3254	-0.0047	0.0355
6.00	0.8562	0.9775	0.8434	30.36	-0.29	0.4941	-3.2064	-0.0043	0.0330
7.00	0.8559	0.9781	0.8490	29.77	-0.38	0.4857	-3.1195	-0.0056	0.0353
8.01	0.8556	0.9776	0.8530	29.25	-0.35	0.4776	-3.0466	-0.0052	0.0326

(e) $\delta_{v,p} = 14.14°, \delta_{v,y} = 14.14°$

NPR	w_p/w_i	F_r/F_i	F/F_i	δ_p	δ_y	F_N/F_i	PM/$F_i l$	F_Y/F_i	YM/$F_i l$
1.51	0.8538	0.9584	0.9400	7.94	8.06	0.1311	-0.9905	0.1331	-0.9586
2.01	0.8939	0.9673	0.9433	9.18	9.06	0.1524	-1.0731	0.1505	-1.0502
2.51	0.9190	0.9705	0.9345	11.36	11.05	0.1878	-1.2855	0.1826	-1.2756
3.01	0.9258	0.9729	0.9248	13.15	12.88	0.2161	-1.4779	0.2115	-1.4653
3.50	0.9211	0.9681	0.8852	17.68	17.11	0.2821	-1.9328	0.2724	-1.8943
4.01	0.9217	0.9748	0.8899	17.85	17.25	0.2865	-1.9583	0.2763	-1.9223
5.00	0.9217	0.9799	0.9014	17.06	16.49	0.2766	-1.8641	0.2669	-1.8332
6.00	0.9205	0.9804	0.9064	16.52	15.99	0.2688	-1.7917	0.2597	-1.7619
7.00	0.9197	0.9788	0.9078	16.17	15.63	0.2632	-1.7388	0.2540	-1.7096
8.01	0.9193	0.9764	0.9079	15.92	15.35	0.2589	-1.6976	0.2492	-1.6685

Table 3. Static Characteristics for Dry Power Nozzle With Long Flap

(a) $\delta_{v,p} = 0°, \delta_{v,y} = 0°$

NPR	w_p/w_i	F_r/F_i	F/F_i	δ_p	δ_y	F_N/F_i	PM/$F_i l$	F_Y/F_i	YM/$F_i l$
1.50	0.9903	0.8399	0.8399	-0.15	-0.87	-0.0023	-0.0579	-0.0127	0.0690
2.00	0.9476	0.9109	0.9109	-0.24	-0.46	-0.0038	0.0101	-0.0073	0.0362
2.51	0.9436	0.9397	0.9397	-0.14	-0.30	-0.0023	0.0156	-0.0048	0.0210
2.99	0.9479	0.9577	0.9577	0.02	-0.25	0.0003	0.0121	-0.0042	0.0090
3.51	0.9436	0.9674	0.9674	0.14	-0.23	0.0024	0.0072	-0.0039	0.0072
4.01	0.9442	0.9756	0.9756	0.20	-0.15	0.0035	0.0016	-0.0026	0.0044
5.00	0.9434	0.9836	0.9836	0.22	-0.17	0.0037	-0.0040	-0.0029	0.0056
5.99	0.9433	0.9843	0.9843	0.18	-0.13	0.0031	-0.0081	-0.0022	0.0058
7.00	0.9426	0.9830	0.9830	0.15	-0.14	0.0026	-0.0104	-0.0024	0.0092
8.01	0.9421	0.9818	0.9818	0.15	-0.12	0.0026	-0.0115	-0.0021	0.0082

(b) $\delta_{v,p} = 10°, \delta_{v,y} = 0°$

NPR	w_p/w_i	F_r/F_i	F/F_i	δ_p	δ_y	F_N/F_i	PM/$F_i l$	F_Y/F_i	YM/$F_i l$
1.50	0.9581	0.9094	0.9026	7.05	-0.31	0.1115	-0.9082	-0.0049	0.0128
2.00	0.9446	0.9113	0.9008	8.72	-0.33	0.1382	-0.9657	-0.0052	0.0244
2.50	0.9456	0.9401	0.9081	14.98	-0.45	0.2430	-1.6769	-0.0072	0.0365
3.00	0.9448	0.9574	0.9281	14.22	-0.27	0.2352	-1.6139	-0.0044	0.0168
3.51	0.9465	0.9695	0.9443	13.11	-0.23	0.2200	-1.4960	-0.0037	0.0159
4.00	0.9460	0.9779	0.9549	12.44	-0.22	0.2107	-1.4257	-0.0037	0.0163
5.01	0.9460	0.9845	0.9637	11.80	-0.18	0.2013	-1.3368	-0.0031	0.0141
6.00	0.9458	0.9848	0.9652	11.45	-0.16	0.1955	-1.2795	-0.0027	0.0136
7.01	0.9441	0.9839	0.9652	11.19	-0.14	0.1909	-1.2362	-0.0023	0.0157
7.99	0.9439	0.9829	0.9646	11.08	-0.15	0.1889	-1.2050	-0.0024	0.0148

Table 3. Concluded

(c) $\delta_{v,p} = 20°, \delta_{v,y} = 0°$

NPR	w_p/w_i	F_r/F_i	F/F_i	δ_p	δ_y	F_N/F_i	PM/$F_i l$	F_Y/F_i	YM/$F_i l$
1.50	0.8638	0.9212	0.8794	17.32	-0.54	0.2742	-2.0419	-0.0084	0.0246
2.00	0.8928	0.9412	0.9064	15.64	-0.29	0.2538	-1.7721	-0.0046	0.0036
2.50	0.9087	0.9374	0.8443	25.76	-0.34	0.4074	-2.7999	-0.0050	0.0233
3.01	0.9092	0.9590	0.8670	25.30	-0.33	0.4098	-2.7970	-0.0050	0.0269
3.50	0.9095	0.9711	0.8884	23.81	-0.29	0.3921	-2.6459	-0.0044	0.0260
4.00	0.9095	0.9783	0.9012	22.90	-0.29	0.3807	-2.5353	-0.0045	0.0245
5.01	0.9097	0.9855	0.9158	21.68	-0.20	0.3640	-2.3773	-0.0033	0.0227
6.01	0.9097	0.9871	0.9217	20.98	-0.19	0.3534	-2.2764	-0.0030	0.0221
7.00	0.9088	0.9864	0.9235	20.57	-0.21	0.3466	-2.2011	-0.0033	0.0228
8.00	0.9083	0.9856	0.9249	20.23	-0.24	0.3407	-2.1449	-0.0039	0.0209

(d) $\delta_{v,p} = 30°, \delta_{v,y} = 0°$

NPR	w_p/w_i	F_r/F_i	F/F_i	δ_p	δ_y	F_N/F_i	PM/$F_i l$	F_Y/F_i	YM/$F_i l$
1.51	0.7810	0.9152	0.7956	29.62	-0.54	0.4523	-3.1856	-0.0075	0.0405
2.01	0.8237	0.9301	0.8191	28.28	-0.34	0.4406	-2.9913	-0.0049	0.0224
2.51	0.8406	0.9394	0.7919	32.55	-0.40	0.5054	-3.4193	-0.0055	0.0241
3.01	0.8410	0.9598	0.7775	35.90	-0.52	0.5628	-3.8019	-0.0070	0.0448
3.51	0.8372	0.9691	0.8019	34.16	-0.41	0.5442	-3.6460	-0.0057	0.0391
4.01	0.8370	0.9769	0.8222	32.69	-0.33	0.5277	-3.4985	-0.0048	0.0355
5.01	0.8371	0.9856	0.8456	30.91	-0.30	0.5063	-3.2881	-0.0045	0.0334
6.03	0.8374	0.9873	0.8565	29.83	-0.27	0.4912	-3.1442	-0.0041	0.0280
7.00	0.8367	0.9881	0.8629	29.15	-0.29	0.4813	-3.0435	-0.0043	0.0277
8.00	0.8366	0.9877	0.8670	28.62	-0.31	0.4731	-2.9647	-0.0047	0.0260

Table 4. Static Characteristics for A/B Power Nozzle With Short Flap

(a) $\delta_{v,p} = 0°, \delta_{v,y} = 0°$

NPR	w_p/w_i	F_r/F_i	F/F_i	δ_p	δ_y	F_N/F_i	PM/$F_i l$	F_Y/F_i	YM/$F_i l$
1.50	1.0305	0.8957	0.8957	0.30	-0.15	0.0047	-0.0112	-0.0023	-0.0054
2.01	0.9877	0.9318	0.9318	0.19	-0.01	0.0031	0.0099	-0.0001	-0.0120
2.50	0.9889	0.9466	0.9465	0.33	0.06	0.0055	-0.0028	0.0010	-0.0169
3.00	0.9890	0.9649	0.9648	0.33	0.06	0.0055	-0.0049	0.0010	-0.0150
3.51	0.9890	0.9763	0.9763	0.27	0.10	0.0045	-0.0062	0.0017	-0.0154
4.01	0.9891	0.9826	0.9826	0.23	0.11	0.0039	-0.0079	0.0019	-0.0146
4.99	0.9884	0.9887	0.9887	0.21	0.12	0.0037	-0.0090	0.0021	-0.0148
5.37	0.9882	0.9893	0.9893	0.23	0.11	0.0039	-0.0094	0.0018	-0.0156

(b) $\delta_{v,p} = 10°, \delta_{v,y} = 0°$

NPR	w_p/w_i	F_r/F_i	F/F_i	δ_p	δ_y	F_N/F_i	PM/$F_i l$	F_Y/F_i	YM/$F_i l$
1.50	1.0271	0.9539	0.9533	2.00	-0.11	0.0333	-0.2110	-0.0018	-0.0084
2.00	0.9902	0.9538	0.9536	1.11	-0.34	0.0186	-0.0798	-0.0056	0.0076
2.50	0.9923	0.9598	0.9516	7.52	0.02	0.1256	-0.6428	0.0003	-0.0077
2.99	0.9924	0.9715	0.9585	9.37	0.00	0.1581	-0.8072	0.0000	-0.0083
3.50	0.9921	0.9781	0.9603	10.93	0.03	0.1855	-0.9462	0.0004	-0.0044
4.01	0.9920	0.9830	0.9641	11.26	0.03	0.1919	-0.9732	0.0004	-0.0019
4.99	0.9915	0.9870	0.9691	10.94	0.01	0.1873	-0.9326	0.0002	-0.0028
5.32	0.9913	0.9870	0.9695	10.81	0.01	0.1851	-0.9203	0.0001	-0.0031

(c) $\delta_{v,p} = 20°, \delta_{v,y} = 0°$

NPR	w_p/w_i	F_r/F_i	F/F_i	δ_p	δ_y	F_N/F_i	PM/$F_i l$	F_Y/F_i	YM/$F_i l$
1.50	0.9462	0.9760	0.9651	8.59	-0.48	0.1457	-0.7304	-0.0080	0.0056
2.00	0.9591	0.9844	0.9701	9.77	-0.09	0.1671	-0.8227	-0.0015	-0.0068
2.50	0.9644	0.9802	0.9577	12.28	-0.50	0.2085	-1.0311	-0.0084	0.0355
3.00	0.9647	0.9821	0.9498	14.74	-0.32	0.2499	-1.2376	-0.0054	0.0224
3.51	0.9646	0.9802	0.9346	17.54	-0.22	0.2955	-1.4636	-0.0035	0.0178
4.00	0.9642	0.9814	0.9283	18.93	-0.03	0.3183	-1.5724	-0.0005	0.0010
4.99	0.9636	0.9846	0.9299	19.18	-0.06	0.3235	-1.5819	-0.0010	-0.0002
5.45	0.9636	0.9841	0.9294	19.19	-0.07	0.3234	-1.5824	-0.0011	-0.0010

Table 4. Concluded

(d) $\delta_{v,p} = 30°, \delta_{v,y} = 0°$

NPR	w_p/w_i	F_r/F_i	F/F_i	δ_p	δ_y	F_N/F_i	PM/$F_i l$	F_Y/F_i	YM/$F_i l$
1.50	0.8598	0.9797	0.9428	15.78	-0.36	0.2664	-1.3386	-0.0060	0.0075
2.00	0.8898	0.9832	0.9353	17.97	-0.18	0.3033	-1.4976	-0.0029	0.0099
2.51	0.9040	0.9848	0.9237	20.29	-0.09	0.3415	-1.6768	-0.0014	0.0029
3.00	0.9080	0.9840	0.9155	21.51	-0.16	0.3608	-1.7684	-0.0026	0.0178
3.51	0.9092	0.9824	0.9035	23.11	-0.33	0.3856	-1.8786	-0.0051	0.0276
4.01	0.9090	0.9820	0.8963	24.12	-0.24	0.4013	-1.9446	-0.0038	0.0186
5.01	0.9084	0.9805	0.8834	25.71	-0.12	0.4254	-2.0522	-0.0018	0.0051
5.69	0.9074	0.9796	0.8815	25.86	-0.15	0.4273	-2.0589	-0.0023	0.0066

(e) $\delta_{v,p} = 7.07°, \delta_{v,y} = 7.07°$

NPR	w_p/w_i	F_r/F_i	F/F_i	δ_p	δ_y	F_N/F_i	PM/$F_i l$	F_Y/F_i	YM/$F_i l$
1.51	1.0212	0.9580	0.9577	0.71	1.21	0.0119	-0.0880	0.0203	-0.1684
2.00	0.9893	0.9489	0.9481	1.87	1.40	0.0310	-0.1420	0.0233	-0.1735
2.50	0.9906	0.9632	0.9565	4.78	4.78	0.0801	-0.4045	0.0800	-0.4395
3.01	0.9911	0.9739	0.9619	6.47	6.29	0.1091	-0.5569	0.1061	-0.5630
3.51	0.9917	0.9794	0.9624	7.75	7.48	0.1309	-0.6722	0.1263	-0.6568
4.00	0.9924	0.9832	0.9649	8.01	7.75	0.1358	-0.6930	0.1312	-0.6740
5.00	0.9915	0.9865	0.9690	7.82	7.58	0.1331	-0.6701	0.1289	-0.6489
5.32	0.9915	0.9864	0.9693	7.74	7.49	0.1318	-0.6622	0.1275	-0.6407

(f) $\delta_{v,p} = 14.14°, \delta_{v,y} = 14.14°$

NPR	w_p/w_i	F_r/F_i	F/F_i	δ_p	δ_y	F_N/F_i	PM/$F_i l$	F_Y/F_i	YM/$F_i l$
1.50	0.9464	0.9794	0.9695	5.90	5.67	0.1001	-0.5159	0.0962	-0.5189
2.01	0.9598	0.9788	0.9647	7.34	6.44	0.1243	-0.6135	0.1089	-0.5778
2.50	0.9632	0.9817	0.9613	8.90	7.69	0.1505	-0.7516	0.1298	-0.6666
3.00	0.9639	0.9753	0.9367	12.02	11.13	0.1994	-1.0002	0.1844	-0.9436
3.50	0.9636	0.9798	0.9351	12.70	12.24	0.2107	-1.0525	0.2028	-1.0302
4.00	0.9639	0.9812	0.9321	13.32	12.85	0.2207	-1.0971	0.2126	-1.0662
5.00	0.9639	0.9826	0.9286	13.98	13.52	0.2313	-1.1437	0.2232	-1.1085
5.40	0.9637	0.9822	0.9282	14.01	13.50	0.2315	-1.1408	0.2228	-1.1053

Table 5. Static Characteristics for A/B Power Nozzle With Long Flap

(a) $\delta_{v,p} = 0°, \delta_{v,y} = 0°$

NPR	w_p/w_i	F_r/F_i	F/F_i	δ_p	δ_y	F_N/F_i	PM/$F_i l$	F_Y/F_i	YM/$F_i l$
1.50	1.0326	0.8967	0.8960	-1.82	-1.34	-0.0284	0.1598	-0.0209	0.0881
2.00	0.9883	0.9373	0.9373	-0.07	-0.12	-0.0011	0.0279	-0.0020	-0.0014
2.50	0.9895	0.9566	0.9566	0.24	0.12	0.0040	0.0062	0.0020	-0.0213
3.00	0.9898	0.9699	0.9699	0.30	0.10	0.0050	-0.0071	0.0017	-0.0163
3.50	0.9898	0.9801	0.9801	0.28	0.14	0.0047	-0.0094	0.0023	-0.0192
4.00	0.9908	0.9861	0.9861	0.25	0.14	0.0042	-0.0114	0.0024	-0.0179
5.01	0.9900	0.9911	0.9911	0.27	0.15	0.0046	-0.0118	0.0025	-0.0180
5.59	0.9890	0.9917	0.9917	0.26	0.11	0.0045	-0.0119	0.0020	-0.0177

(b) $\delta_{v,p} = 10°, \delta_{v,y} = 0°$

NPR	w_p/w_i	F_r/F_i	F/F_i	δ_p	δ_y	F_N/F_i	PM/$F_i l$	F_Y/F_i	YM/$F_i l$
1.50	1.0216	0.9402	0.9347	6.12	-0.57	0.1003	-0.5522	-0.0094	0.0216
2.01	0.9848	0.9447	0.9410	5.07	-0.14	0.0836	-0.4018	-0.0022	0.0009
2.50	0.9855	0.9602	0.9461	9.81	0.04	0.1637	-0.8208	0.0006	-0.0151
3.01	0.9857	0.9759	0.9435	14.82	0.05	0.2496	-1.2887	0.0008	-0.0073
3.51	0.9861	0.9856	0.9548	14.36	0.04	0.2444	-1.2506	0.0006	-0.0060
4.00	0.9863	0.9909	0.9619	13.90	0.07	0.2380	-1.2041	0.0011	-0.0073
5.00	0.9858	0.9951	0.9687	13.24	0.06	0.2278	-1.1360	0.0010	-0.0086
5.51	0.9851	0.9954	0.9699	13.00	0.04	0.2239	-1.1112	0.0007	-0.0094

(c) $\delta_{v,p} = 20°, \delta_{v,y} = 0°$

NPR	w_p/w_i	F_r/F_i	F/F_i	δ_p	δ_y	F_N/F_i	PM/$F_i l$	F_Y/F_i	YM/$F_i l$
1.51	0.9313	0.9612	0.9323	14.08	-0.43	0.2339	-1.2119	-0.0069	0.0063
2.00	0.9411	0.9737	0.9440	14.17	-0.29	0.2384	-1.2022	-0.0048	0.0106
2.50	0.9490	0.9780	0.9365	16.75	-0.15	0.2818	-1.4184	-0.0024	0.0054
3.00	0.9498	0.9810	0.8803	26.19	-0.01	0.4330	-2.2015	-0.0002	-0.0035
3.51	0.9497	0.9898	0.8958	25.18	0.02	0.4211	-2.1217	0.0004	-0.0059
4.00	0.9494	0.9945	0.9062	24.32	0.01	0.4096	-2.0417	0.0002	-0.0056
5.00	0.9490	0.9990	0.9190	23.08	-0.03	0.3916	-1.9268	-0.0005	-0.0058
5.64	0.9491	0.9981	0.9220	22.52	-0.04	0.3823	-1.8752	-0.0007	-0.0057

(d) $\delta_{v,p} = 30°, \delta_{v,y} = 0°$

NPR	w_p/w_i	F_r/F_i	F/F_i	δ_p	δ_y	F_N/F_i	PM/$F_i l$	F_Y/F_i	YM/$F_i l$
1.50	0.8339	0.9637	0.8764	24.57	-0.19	0.4006	-2.0138	-0.0030	0.0004
2.00	0.8646	0.9707	0.8746	25.71	-0.03	0.4212	-2.0997	-0.0005	-0.0005
2.50	0.8785	0.9758	0.8590	28.33	-0.06	0.4630	-2.3077	-0.0009	0.0089
3.00	0.8803	0.9827	0.7940	36.10	-0.20	0.5790	-2.9102	-0.0028	0.0198
3.51	0.8802	0.9902	0.8159	34.51	-0.18	0.5610	-2.7901	-0.0026	0.0149
4.01	0.8803	0.9947	0.8328	33.15	-0.15	0.5440	-2.6783	-0.0021	0.0130
5.01	0.8801	0.9979	0.8521	31.37	-0.14	0.5194	-2.5215	-0.0021	0.0103
5.39	0.8794	0.9986	0.8568	30.90	-0.15	0.5128	-2.4795	-0.0023	0.0092

Table 6. Internal Static Pressure Ratios With Dry Power, Short Flap, and $\delta_{v,p} = 0°$

$\phi = 0°$

NPR	Internal static pressure ratio for x/L_f of—						
	-0.025	0.145	0.285	0.430	0.570	0.715	0.860
1.507	0.702	0.397	0.469	0.532	0.576	0.610	0.635
2.019	0.698	0.232	0.297	0.299	0.285	0.439	0.462
2.500	0.702	0.233	0.296	0.295	0.283	0.246	0.248
2.997	0.701	0.233	0.295	0.295	0.283	0.246	0.226
3.494	0.704	0.235	0.294	0.292	0.282	0.246	0.228
4.002	0.699	0.233	0.295	0.295	0.283	0.245	0.225
4.993	0.697	0.231	0.293	0.296	0.284	0.244	0.223
6.003	0.698	0.231	0.292	0.295	0.284	0.244	0.222
6.990	0.698	0.231	0.292	0.294	0.284	0.243	0.221
8.013	0.699	0.231	0.292	0.293	0.284	0.243	0.220

$\phi = 45°$

NPR	Internal static pressure ratio for x/L_f of—			
	0.200	0.400	0.600	0.800
1.507	0.419	0.521	0.586	0.627
2.019	0.278	0.314	0.281	0.455
2.500	0.282	0.315	0.270	0.229
2.997	0.280	0.312	0.268	0.228
3.494	0.283	0.314	0.268	0.229
4.002	0.279	0.309	0.266	0.228
4.993	0.278	0.306	0.263	0.227
6.003	0.278	0.306	0.263	0.227
6.990	0.277	0.305	0.262	0.226
8.013	0.277	0.304	0.261	0.226

$\phi = 90°$

NPR	Internal static pressure ratio for x/L_f of—						
	-0.025	0.145	0.285	0.430	0.570	0.715	0.860
1.507	0.707	0.384	0.466	0.532	0.579	0.611	0.637
2.019	0.703	0.230	0.301	0.303	0.278	0.442	0.463
2.500	0.705	0.232	0.297	0.302	0.278	0.250	0.272
2.997	0.704	0.234	0.297	0.300	0.275	0.248	0.214
3.494	0.706	0.235	0.295	0.300	0.277	0.250	0.215
4.002	0.702	0.236	0.296	0.298	0.273	0.247	0.212
4.993	0.700	0.234	0.295	0.297	0.272	0.246	0.211
6.003	0.700	0.233	0.295	0.297	0.272	0.246	0.210
6.990	0.699	0.233	0.295	0.298	0.271	0.246	0.209
8.013	0.699	0.233	0.294	0.297	0.271	0.246	0.208

Table 6. Concluded

$\phi = 135°$

NPR	Internal static pressure ratio for x/L_f of—				
	0.165	0.330	0.500	0.670	0.835
1.507	0.382	0.487	0.558	0.604	0.634
2.019	0.245	0.294	0.287	0.411	0.459
2.500	0.252	0.297	0.287	0.259	0.227
2.997	0.253	0.297	0.286	0.259	0.225
3.494	0.260	0.298	0.285	0.258	0.223
4.002	0.260	0.296	0.284	0.258	0.224
4.993	0.261	0.295	0.283	0.258	0.225
6.003	0.257	0.294	0.283	0.259	0.225
6.990	0.259	0.294	0.283	0.259	0.225
8.013	0.255	0.293	0.282	0.258	0.225

$\phi = 180°$

NPR	Internal static pressure ratio for x/L_f of—						
	-0.025	0.145	0.285	0.430	0.570	0.715	0.860
1.507	0.703	0.321	0.656	0.542	0.587	0.617	0.640
2.019	0.702	0.201	0.490	0.298	0.264	0.444	0.463
2.500	0.706	0.226	0.396	0.297	0.262	0.236	0.296
2.997	0.706	0.227	0.330	0.296	0.260	0.236	0.214
3.494	0.708	0.233	0.283	0.296	0.259	0.237	0.214
4.002	0.706	0.235	0.247	0.295	0.257	0.235	0.213
4.993	0.705	0.236	0.198	0.294	0.256	0.235	0.213
6.003	0.705	0.234	0.165	0.294	0.255	0.234	0.212
6.990	0.703	0.236	0.142	0.293	0.254	0.233	0.212
8.013	0.702	0.234	0.124	0.293	0.253	0.233	0.211

Table 7. Internal Static Pressure Ratios With Dry Power, Short Flap, and $\delta_{v,p} = 10°$

$\phi = 0°$

	Internal static pressure ratio for x/L_f of—						
NPR	-0.025	0.145	0.285	0.430	0.570	0.715	0.860
1.496	0.683	0.676	0.675	0.660	0.654	0.652	0.654
1.995	0.653	0.597	0.562	0.509	0.469	0.438	0.432
2.497	0.652	0.561	0.524	0.455	0.402	0.353	0.311
3.007	0.654	0.556	0.525	0.452	0.396	0.341	0.291
3.509	0.651	0.555	0.522	0.449	0.394	0.339	0.290
4.007	0.652	0.554	0.522	0.449	0.393	0.339	0.289
4.996	0.652	0.552	0.522	0.449	0.393	0.339	0.288
5.996	0.650	0.551	0.520	0.448	0.393	0.338	0.288
6.997	0.652	0.550	0.522	0.449	0.394	0.338	0.287
8.004	0.651	0.554	0.519	0.447	0.393	0.337	0.287

$\phi = 45°$

	Internal static pressure ratio for x/L_f of—			
NPR	0.200	0.400	0.600	0.800
1.496	0.668	0.654	0.649	0.645
1.995	0.571	0.502	0.461	0.430
2.497	0.519	0.448	0.391	0.317
3.007	0.518	0.436	0.371	0.292
3.509	0.514	0.435	0.369	0.290
4.007	0.513	0.434	0.368	0.289
4.996	0.511	0.434	0.367	0.289
5.996	0.511	0.433	0.366	0.288
6.997	0.513	0.433	0.365	0.287
8.004	0.509	0.432	0.365	0.287

$\phi = 90°$

	Internal static pressure ratio for x/L_f of—						
NPR	-0.025	0.145	0.285	0.430	0.570	0.715	0.860
1.496	0.721	0.562	0.599	0.623	0.634	0.644	0.654
1.995	0.690	0.397	0.466	0.476	0.472	0.470	0.477
2.497	0.686	0.256	0.387	0.410	0.369	0.335	0.315
3.007	0.687	0.235	0.316	0.377	0.323	0.277	0.238
3.509	0.685	0.235	0.315	0.373	0.321	0.276	0.238
4.007	0.685	0.233	0.312	0.371	0.320	0.276	0.238
4.996	0.685	0.232	0.312	0.370	0.320	0.275	0.237
5.996	0.685	0.231	0.311	0.370	0.319	0.275	0.236
6.997	0.687	0.230	0.303	0.372	0.320	0.275	0.236
8.004	0.686	0.230	0.311	0.368	0.319	0.275	0.235

Table 7. Concluded

$\phi = 135°$

Internal static pressure ratio for x/L_f of—

NPR	0.165	0.330	0.500	0.670	0.835
1.496	0.600	0.587	0.600	0.613	0.631
1.995	0.452	0.440	0.444	0.451	0.463
2.497	0.254	0.303	0.334	0.351	0.363
3.007	0.166	0.198	0.191	0.240	0.296
3.509	0.165	0.199	0.190	0.213	0.213
4.007	0.168	0.200	0.191	0.211	0.212
4.996	0.167	0.200	0.190	0.211	0.212
5.996	0.166	0.199	0.189	0.209	0.212
6.997	0.167	0.199	0.189	0.207	0.212
8.004	0.167	0.199	0.188	0.208	0.211

$\phi = 180°$

Internal static pressure ratio for x/L_f of—

NPR	-0.025	0.145	0.285	0.430	0.570	0.715	0.860
1.496	0.751	0.633	0.610	0.606	0.610	0.622	0.634
1.995	0.704	0.475	0.461	0.458	0.461	0.467	0.471
2.497	0.693	0.307	0.320	0.335	0.346	0.355	0.365
3.007	0.694	0.121	0.159	0.164	0.282	0.303	0.311
3.509	0.694	0.121	0.158	0.163	0.152	0.142	0.262
4.007	0.694	0.123	0.157	0.162	0.151	0.140	0.127
4.996	0.694	0.124	0.157	0.162	0.151	0.140	0.126
5.996	0.693	0.124	0.158	0.163	0.150	0.140	0.125
6.997	0.692	0.126	0.158	0.162	0.150	0.140	0.124
8.004	0.691	0.125	0.157	0.162	0.149	0.139	0.123

Table 8. Internal Static Pressure Ratios With Dry Power, Short Flap, and $\delta_{v,p} = 20°$

$\phi = 0°$

	Internal static pressure ratio for x/L_f of—						
NPR	-0.025	0.145	0.285	0.430	0.570	0.715	0.860
1.496	0.797	0.803	0.780	0.746	0.720	0.696	0.666
2.003	0.739	0.739	0.701	0.641	0.593	0.544	0.483
2.498	0.721	0.718	0.673	0.602	0.542	0.482	0.411
2.997	0.709	0.706	0.657	0.583	0.519	0.457	0.380
3.505	0.706	0.703	0.652	0.573	0.506	0.440	0.360
4.008	0.706	0.702	0.651	0.572	0.506	0.439	0.358
5.024	0.705	0.702	0.651	0.573	0.506	0.439	0.357
6.024	0.705	0.702	0.651	0.574	0.505	0.439	0.356
7.007	0.705	0.702	0.651	0.576	0.506	0.440	0.356
8.002	0.704	0.702	0.650	0.575	0.505	0.440	0.356

$\phi = 45°$

	Internal static pressure ratio for x/L_f of—			
NPR	0.200	0.400	0.600	0.800
1.496	0.765	0.733	0.698	0.667
2.003	0.682	0.620	0.551	0.490
2.498	0.651	0.574	0.490	0.412
2.997	0.632	0.551	0.462	0.377
3.505	0.624	0.536	0.449	0.360
4.008	0.623	0.535	0.444	0.350
5.024	0.623	0.535	0.443	0.350
6.024	0.623	0.535	0.444	0.349
7.007	0.623	0.536	0.444	0.349
8.002	0.622	0.536	0.444	0.349

$\phi = 90°$

	Internal static pressure ratio for x/L_f of—						
NPR	-0.025	0.145	0.285	0.430	0.570	0.715	0.860
1.496	0.769	0.633	0.665	0.672	0.669	0.659	0.655
2.003	0.719	0.470	0.533	0.531	0.512	0.487	0.469
2.498	0.710	0.410	0.496	0.472	0.435	0.397	0.372
2.997	0.706	0.440	0.475	0.427	0.389	0.346	0.312
3.505	0.704	0.418	0.463	0.417	0.361	0.313	0.279
4.008	0.704	0.412	0.447	0.393	0.345	0.296	0.256
5.024	0.704	0.397	0.452	0.394	0.345	0.295	0.256
6.024	0.704	0.381	0.454	0.392	0.344	0.294	0.255
7.007	0.704	0.373	0.458	0.394	0.345	0.294	0.255
8.002	0.703	0.366	0.456	0.392	0.344	0.294	0.255

Table 8. Concluded

$\phi = 135°$

NPR	Internal static pressure ratio for x/L_f of—				
	0.165	0.330	0.500	0.670	0.835
1.496	0.633	0.629	0.628	0.630	0.637
2.003	0.465	0.458	0.455	0.456	0.462
2.498	0.356	0.351	0.348	0.350	0.361
2.997	0.258	0.261	0.274	0.288	0.299
3.505	0.181	0.210	0.233	0.233	0.234
4.008	0.095	0.135	0.209	0.227	0.201
5.024	0.097	0.135	0.204	0.225	0.202
6.024	0.099	0.139	0.199	0.221	0.202
7.007	0.102	0.142	0.197	0.219	0.202
8.002	0.102	0.160	0.194	0.215	0.203

$\phi = 180°$

NPR	Internal static pressure ratio for x/L_f of—						
	-0.025	0.145	0.285	0.430	0.570	0.715	0.860
1.496	0.771	0.650	0.644	0.642	0.642	0.645	0.644
2.003	0.708	0.481	0.475	0.470	0.470	0.473	0.472
2.498	0.697	0.377	0.365	0.357	0.357	0.366	0.372
2.997	0.692	0.294	0.282	0.280	0.285	0.293	0.308
3.505	0.691	0.213	0.200	0.203	0.214	0.227	0.247
4.008	0.691	0.062	0.086	0.095	0.096	0.186	0.201
5.024	0.691	0.062	0.087	0.095	0.096	0.098	0.201
6.024	0.689	0.062	0.087	0.095	0.095	0.098	0.201
7.007	0.688	0.062	0.087	0.095	0.095	0.100	0.202
8.002	0.687	0.063	0.088	0.095	0.095	0.108	0.203

Table 9. Internal Static Pressure Ratios With Dry Power, Short Flap, and $\delta_{v,p} = 30°$

$\phi = 0°$

NPR	Internal static pressure ratio for x/L_f of—						
	-0.025	0.145	0.285	0.430	0.570	0.715	0.860
1.506	0.897	0.883	0.850	0.815	0.777		0.699
1.997	0.868	0.848	0.802	0.746	0.688		0.568
2.501	0.857	0.834	0.780	0.716	0.648		0.518
3.005	0.853	0.828	0.771	0.702	0.626		0.481
3.502	0.849	0.825	0.767	0.696	0.619		0.466
4.000	0.848	0.824	0.767	0.696	0.619		0.463
4.998	0.847	0.823	0.766	0.696	0.618		0.462
6.002	0.847	0.823	0.765	0.696	0.619		0.462
6.999	0.846	0.823	0.765	0.696	0.619		0.462
8.005	0.846	0.823	0.765	0.697	0.619		0.463

$\phi = 45°$

NPR	Internal static pressure ratio for x/L_f of—			
	0.200	0.400	0.600	0.800
1.506	0.839	0.791	0.743	0.693
1.997	0.783	0.709	0.631	0.549
2.501	0.756	0.669	0.584	0.494
3.005	0.747	0.649	0.552	0.457
3.502	0.743	0.644	0.539	0.433
4.000	0.743	0.643	0.535	0.425
4.998	0.742	0.644	0.535	0.424
6.002	0.742	0.644	0.534	0.424
6.999	0.742	0.644	0.534	0.424
8.005	0.742	0.643	0.534	0.424

$\phi = 90°$

NPR	Internal static pressure ratio for x/L_f of—						
	-0.025	0.145	0.285	0.430	0.570	0.715	0.860
1.506	0.787	0.724	0.729	0.712	0.686	0.668	0.658
1.997	0.740	0.636	0.623	0.583	0.537	0.500	0.482
2.501	0.728	0.481	0.599	0.550	0.474	0.434	0.413
3.005	0.725	0.448	0.544	0.514	0.449	0.385	0.346
3.502	0.721	0.480	0.519	0.472	0.408	0.353	0.315
4.000	0.722	0.478	0.519	0.457	0.391	0.333	0.291
4.998	0.722	0.502	0.512	0.453	0.384	0.324	0.280
6.002	0.722	0.465	0.516	0.454	0.385	0.325	0.281
6.999	0.722	0.489	0.511	0.453	0.384	0.324	0.280
8.005	0.722	0.497	0.509	0.453	0.384	0.324	0.280

Table 9. Concluded

$\phi = 135°$

NPR	Internal static pressure ratio for x/L_f of—				
	0.165	0.330	0.500	0.670	0.835
1.506	0.636	0.632	0.628	0.627	0.631
1.997	0.452	0.446	0.443	0.448	0.459
2.501	0.327	0.333	0.353	0.362	0.366
3.005	0.240	0.259	0.280	0.300	0.307
3.502	0.187	0.180	0.207	0.253	0.281
4.000	0.120	0.143	0.170	0.276	0.271
4.998	0.113	0.146	0.168	0.235	0.243
6.002	0.111	0.152	0.177	0.227	0.236
6.999	0.109	0.157	0.182	0.227	0.232
8.005	0.111	0.163	0.181	0.216	0.229

$\phi = 180°$

NPR	Internal static pressure ratio for x/L_f of—						
	-0.025	0.145	0.285	0.430	0.570	0.715	0.860
1.506	0.785	0.651	0.641	0.637	0.636	0.640	0.639
1.997	0.729	0.470	0.455	0.447	0.448	0.461	0.474
2.501	0.717	0.356	0.353	0.354	0.355	0.360	0.376
3.005	0.715	0.275	0.277	0.285	0.290	0.293	0.302
3.502	0.712	0.196	0.194	0.216	0.240	0.253	0.261
4.000	0.711	0.127	0.137	0.168	0.207	0.230	0.242
4.998	0.711	0.075	0.101	0.127	0.161	0.206	0.234
6.002	0.710	0.070	0.095	0.121	0.154	0.200	0.229
6.999	0.710	0.051	0.090	0.118	0.152	0.200	0.233
8.005	0.709	0.043	0.089	0.118	0.152	0.203	0.238

Table 10. Internal Static Pressure Ratios With Dry Power, Long Flap, and $\delta_{v,p} = 0°$

$\phi = 0°$

NPR	Internal static pressure ratio for x/L_f of—						
	-0.025	0.145	0.285	0.430	0.570	0.715	0.860
1.498	0.713	0.320	0.336	0.420	0.527	0.580	0.626
2.003	0.713	0.320	0.337	0.295	0.260	0.426	0.453
2.510	0.709	0.318	0.340	0.292	0.252	0.211	0.365
2.989	0.714	0.320	0.335	0.292	0.255	0.211	0.181
3.511	0.709	0.316	0.339	0.291	0.252	0.209	0.179
4.013	0.710	0.316	0.339	0.291	0.253	0.209	0.179
5.000	0.710	0.315	0.338	0.290	0.252	0.208	0.178
5.995	0.710	0.314	0.338	0.289	0.252	0.209	0.177
6.996	0.710	0.314	0.337	0.289	0.252	0.208	0.175
8.008	0.710	0.314	0.337	0.289	0.252	0.208	0.175

$\phi = 45°$

NPR	Internal static pressure ratio for x/L_f of—			
	0.200	0.400	0.600	0.800
1.498	0.343	0.401	0.534	0.602
2.003	0.342	0.312	0.335	0.441
2.510	0.337	0.307	0.240	0.346
2.989	0.343	0.309	0.237	0.193
3.511	0.337	0.305	0.238	0.194
4.013	0.339	0.306	0.237	0.192
5.000	0.339	0.304	0.235	0.193
5.995	0.339	0.304	0.235	0.192
6.996	0.338	0.303	0.234	0.193
8.008	0.338	0.303	0.233	0.192

$\phi = 90°$

NPR	Internal static pressure ratio for x/L_f of—						
	-0.025	0.145	0.285	0.430	0.570	0.715	0.860
1.498	0.688	0.302	0.349	0.432	0.527	0.575	0.624
2.003	0.687	0.305	0.348	0.310	0.282	0.428	0.452
2.510	0.684	0.309	0.345	0.308	0.247	0.212	0.365
2.989	0.688	0.307	0.347	0.312	0.249	0.211	0.181
3.511	0.684	0.306	0.343	0.309	0.245	0.208	0.182
4.013	0.685	0.305	0.343	0.308	0.245	0.208	0.182
5.000	0.685	0.302	0.342	0.311	0.245	0.207	0.180
5.995	0.684	0.301	0.342	0.310	0.245	0.208	0.179
6.996	0.684	0.300	0.341	0.311	0.244	0.207	0.179
8.008	0.684	0.300	0.341	0.311	0.244	0.207	0.179

Table 10. Concluded

$\phi = 135°$

NPR	Internal static pressure ratio for x/L_f of—				
	0.165	0.330	0.500	0.670	0.835
1.498	0.331	0.326	0.497	0.559	0.621
2.003	0.333	0.325	0.275	0.415	0.448
2.510	0.331	0.323	0.275	0.225	0.362
2.989	0.332	0.325	0.273	0.227	0.181
3.511	0.330	0.322	0.273	0.224	0.179
4.013	0.328	0.322	0.271	0.225	0.178
5.000	0.330	0.321	0.271	0.224	0.178
5.995	0.328	0.322	0.271	0.223	0.177
6.996	0.329	0.321	0.271	0.223	0.176
8.008	0.329	0.320	0.271	0.223	0.176

$\phi = 180°$

NPR	Internal static pressure ratio for x/L_f of—						
	-0.025	0.145	0.285	0.430	0.570	0.715	0.860
1.498	0.702	0.318	0.350	0.415	0.521	0.575	0.629
2.003	0.702	0.314	0.350	0.294	0.281	0.427	0.454
2.510	0.701	0.309	0.351	0.294	0.255	0.212	0.369
2.989	0.704	0.311	0.351	0.295	0.254	0.208	0.185
3.511	0.702	0.306	0.351	0.295	0.253	0.208	0.181
4.013	0.701	0.308	0.350	0.293	0.252	0.208	0.181
5.000	0.701	0.308	0.349	0.293	0.252	0.207	0.180
5.995	0.701	0.310	0.349	0.293	0.251	0.207	0.180
6.996	0.700	0.308	0.349	0.293	0.251	0.206	0.180
8.008	0.700	0.308	0.349	0.293	0.251	0.206	0.179

Table 11. Internal Static Pressure Ratios With Dry Power, Long Flap, and $\delta_{v,p} = 10°$

$\phi = 0°$

	Internal static pressure ratio for x/L_f of—						
NPR	-0.025	0.145	0.285	0.430	0.570	0.715	0.860
1.500	0.675	0.650	0.624	0.608	0.610	0.620	0.632
2.003	0.653	0.571	0.497	0.421	0.339	0.288	0.434
2.500	0.650	0.567	0.493	0.414	0.328	0.262	0.242
3.004	0.648	0.565	0.493	0.413	0.328	0.262	0.215
3.509	0.648	0.565	0.494	0.413	0.328	0.262	0.216
4.004	0.648	0.563	0.494	0.413	0.328	0.261	0.215
5.008	0.647	0.562	0.493	0.413	0.327	0.261	0.214
6.000	0.646	0.561	0.493	0.413	0.327	0.261	0.213
7.009	0.644	0.558	0.492	0.412	0.327	0.260	0.212
7.993	0.645	0.559	0.492	0.413	0.327	0.260	0.212

$\phi = 45°$

	Internal static pressure ratio for x/L_f of—			
NPR	0.200	0.400	0.600	0.800
1.500	0.629	0.598	0.616	0.623
2.003	0.521	0.398	0.317	0.423
2.500	0.517	0.388	0.300	0.219
3.004	0.516	0.385	0.299	0.219
3.509	0.516	0.385	0.299	0.218
4.004	0.515	0.383	0.299	0.218
5.008	0.514	0.381	0.299	0.217
6.000	0.513	0.380	0.298	0.216
7.009	0.512	0.379	0.298	0.217
7.993	0.512	0.378	0.298	0.216

$\phi = 90°$

	Internal static pressure ratio for x/L_f of—						
NPR	-0.025	0.145	0.285	0.430	0.570	0.715	0.860
1.500	0.714	0.526	0.585	0.598	0.608	0.625	0.643
2.003	0.699	0.420	0.416	0.356	0.313	0.418	0.467
2.500	0.700	0.395	0.401	0.332	0.270	0.228	0.365
3.004	0.700	0.394	0.399	0.332	0.269	0.228	0.190
3.509	0.699	0.393	0.402	0.332	0.267	0.226	0.190
4.004	0.700	0.389	0.401	0.332	0.267	0.226	0.189
5.008	0.700	0.388	0.400	0.332	0.266	0.225	0.189
6.000	0.699	0.389	0.400	0.331	0.265	0.225	0.188
7.009	0.699	0.390	0.396	0.331	0.266	0.226	0.188
7.993	0.699	0.384	0.397	0.331	0.266	0.225	0.188

Table 11. Concluded

$\phi = 135°$

NPR	Internal static pressure ratio for x/L_f of—				
	0.165	0.330	0.500	0.670	0.835
1.500	0.527	0.552	0.582	0.606	0.631
2.003	0.256	0.357	0.384	0.418	0.451
2.500	0.209	0.289	0.265	0.217	0.365
3.004	0.208	0.288	0.264	0.218	0.208
3.509	0.207	0.287	0.264	0.217	0.193
4.004	0.208	0.285	0.264	0.217	0.195
5.008	0.207	0.284	0.264	0.217	0.192
6.000	0.206	0.283	0.264	0.216	0.189
7.009	0.205	0.283	0.263	0.216	0.191
7.993	0.205	0.280	0.264	0.216	0.187

$\phi = 180°$

NPR	Internal static pressure ratio for x/L_f of—						
	-0.025	0.145	0.285	0.430	0.570	0.715	0.860
1.500	0.718	0.537	0.531	0.553	0.579	0.605	0.630
2.003	0.687	0.244	0.330	0.367	0.388	0.416	0.447
2.500	0.686	0.158	0.185	0.174	0.278	0.338	0.308
3.004	0.684	0.159	0.185	0.174	0.277	0.337	0.284
3.509	0.684	0.160	0.185	0.175	0.271	0.337	0.283
4.004	0.684	0.160	0.184	0.174	0.271	0.338	0.283
5.008	0.682	0.159	0.183	0.174	0.267	0.338	0.282
6.000	0.681	0.158	0.183	0.174	0.263	0.338	0.281
7.009	0.679	0.157	0.181	0.173	0.263	0.339	0.281
7.993	0.679	0.157	0.181	0.173	0.257	0.340	0.281

Table 12. Internal Static Pressure Ratios With Dry Power, Long Flap, and $\delta_{v,p} = 20°$

$\phi = 0°$

	Internal static pressure ratio for x/L_f of—						
NPR	-0.025	0.145	0.285	0.430	0.570	0.715	0.860
1.499	0.815	0.791	0.740	0.694	0.662	0.646	0.634
2.001	0.773	0.733	0.651	0.567	0.496	0.436	0.396
2.496	0.758	0.709	0.611	0.503	0.411	0.322	0.252
3.005	0.757	0.708	0.611	0.502	0.411	0.322	0.252
3.499	0.756	0.708	0.611	0.502	0.411	0.321	0.251
3.999	0.756	0.708	0.611	0.502	0.411	0.322	0.251
5.010	0.755	0.708	0.611	0.503	0.410	0.322	0.250
6.009	0.755	0.708	0.612	0.503	0.410	0.322	0.249
7.000	0.755	0.708	0.611	0.503	0.410	0.321	0.248
8.004	0.754	0.708	0.611	0.503	0.410	0.321	0.248

$\phi = 45°$

	Internal static pressure ratio for x/L_f of—			
NPR	0.200	0.400	0.600	0.800
1.499	0.747	0.683	0.648	0.643
2.001	0.666	0.550	0.461	0.419
2.496	0.626	0.482	0.355	0.259
3.005	0.626	0.481	0.354	0.260
3.499	0.626	0.481	0.354	0.259
3.999	0.625	0.480	0.353	0.260
5.010	0.625	0.480	0.353	0.259
6.009	0.625	0.481	0.353	0.259
7.000	0.624	0.481	0.353	0.259
8.004	0.624	0.481	0.353	0.259

$\phi = 90°$

	Internal static pressure ratio for x/L_f of—						
NPR	-0.025	0.145	0.285	0.430	0.570	0.715	0.860
1.499	0.747	0.667	0.663	0.643	0.632	0.635	0.644
2.001	0.711	0.565	0.528	0.477	0.449	0.435	0.442
2.496	0.702	0.496	0.434	0.357	0.293	0.238	0.354
3.005	0.703	0.500	0.434	0.357	0.292	0.237	0.200
3.499	0.702	0.499	0.434	0.356	0.292	0.237	0.199
3.999	0.703	0.501	0.434	0.357	0.292	0.237	0.198
5.010	0.703	0.501	0.433	0.357	0.291	0.237	0.198
6.009	0.702	0.500	0.434	0.356	0.290	0.236	0.197
7.000	0.702	0.496	0.433	0.356	0.291	0.236	0.197
8.004	0.702	0.497	0.433	0.356	0.291	0.236	0.197

Table 12. Concluded

$\phi = 135°$

NPR	Internal static pressure ratio for x/L_f of—				
	0.165	0.330	0.500	0.670	0.835
1.499	0.585	0.587	0.599	0.614	0.630
2.001	0.403	0.407	0.425	0.444	0.461
2.496	0.154	0.287	0.247	0.207	0.377
3.005	0.151	0.288	0.248	0.208	0.277
3.499	0.152	0.289	0.247	0.207	0.277
3.999	0.150	0.290	0.248	0.207	0.277
5.010	0.149	0.292	0.247	0.206	0.277
6.009	0.148	0.293	0.248	0.207	0.278
7.000	0.150	0.293	0.247	0.206	0.279
8.004	0.148	0.293	0.248	0.206	0.279

$\phi = 180°$

NPR	Internal static pressure ratio for x/L_f of—						
	-0.025	0.145	0.285	0.430	0.570	0.715	0.860
1.499	0.759	0.606	0.591	0.590	0.600	0.616	0.637
2.001	0.713	0.426	0.409	0.411	0.426	0.442	0.462
2.496	0.708	0.089	0.109	0.234	0.311	0.328	0.368
3.005	0.707	0.083	0.110	0.232	0.310	0.326	0.288
3.499	0.708	0.083	0.108	0.230	0.311	0.325	0.288
3.999	0.708	0.085	0.109	0.229	0.310	0.324	0.287
5.010	0.708	0.086	0.108	0.227	0.310	0.322	0.287
6.009	0.707	0.087	0.109	0.227	0.310	0.321	0.286
7.000	0.706	0.087	0.109	0.226	0.310	0.320	0.286
8.004	0.706	0.086	0.109	0.226	0.310	0.320	0.286

Table 13. Internal Static Pressure Ratios With Dry Power, Long Flap, and $\delta_{v,p} = 30°$

$\phi = 0°$

	Internal static pressure ratio for x/L_f of—						
NPR	-0.025	0.145	0.285	0.430	0.570	0.715	0.860
1.509	0.907	0.860	0.804	0.741	0.696	0.662	0.643
2.015	0.886	0.821	0.741	0.640	0.564	0.481	0.420
2.513	0.879	0.807	0.716	0.592	0.495	0.397	0.324
3.012	0.879	0.807	0.714	0.588	0.488	0.378	0.293
3.510	0.874	0.803	0.711	0.585	0.485	0.376	0.291
4.007	0.873	0.802	0.710	0.585	0.485	0.376	0.291
5.007	0.872	0.802	0.711	0.586	0.485	0.375	0.290
6.029	0.873	0.803	0.711	0.587	0.485	0.375	0.290
6.997	0.872	0.802	0.711	0.587	0.485	0.374	0.289
7.997	0.873	0.803	0.712	0.589	0.486	0.374	0.290

$\phi = 45°$

	Internal static pressure ratio for x/L_f of—			
NPR	0.200	0.400	0.600	0.800
1.509	0.809	0.725	0.662	0.639
2.015	0.748	0.615	0.505	0.427
2.513	0.724	0.558	0.430	0.329
3.012	0.723	0.551	0.407	0.292
3.510	0.720	0.548	0.405	0.290
4.007	0.719	0.548	0.405	0.290
5.007	0.719	0.548	0.404	0.290
6.029	0.719	0.549	0.405	0.290
6.997	0.718	0.549	0.404	0.288
7.997	0.718	0.549	0.404	0.288

$\phi = 90°$

	Internal static pressure ratio for x/L_f of—						
NPR	-0.025	0.145	0.285	0.430	0.570	0.715	0.860
1.509		0.733	0.703	0.656	0.633	0.631	0.624
2.015		0.652	0.593	0.502	0.451	0.424	0.425
2.513		0.599	0.538	0.438	0.361	0.287	0.306
3.012		0.597	0.523	0.395	0.322	0.239	0.266
3.510		0.597	0.524	0.392	0.321	0.234	0.263
4.007		0.595	0.525	0.391	0.320	0.236	0.262
5.007		0.590	0.525	0.392	0.320	0.234	0.261
6.029		0.587	0.526	0.392	0.319	0.224	0.258
6.997		0.583	0.531	0.391	0.318	0.223	0.258
7.997		0.582	0.525	0.390	0.317	0.224	0.258

Table 13. Concluded

$\phi = 135°$

NPR	Internal static pressure ratio for x/L_f of—				
	0.165	0.330	0.500	0.670	0.835
1.509	0.575	0.584	0.597	0.610	0.625
2.015	0.364	0.399	0.428	0.449	0.465
2.513	0.204	0.301	0.343	0.336	0.337
3.012	0.162	0.296	0.314	0.273	0.250
3.510	0.163	0.295	0.308	0.268	0.248
4.007	0.162	0.287	0.313	0.268	0.249
5.007	0.160	0.303	0.310	0.267	0.247
6.029	0.161	0.312	0.306	0.268	0.255
6.997	0.163	0.307	0.304	0.271	0.255
7.997	0.163	0.306	0.306	0.271	0.255

$\phi = 180°$

NPR	Internal static pressure ratio for x/L_f of—						
	-0.025	0.145	0.285	0.430	0.570	0.715	0.860
1.509	0.772	0.594	0.585	0.588	0.596	0.608	0.627
2.015	0.729	0.393	0.397	0.414	0.429	0.441	0.453
2.513	0.725	0.250	0.276	0.292	0.311	0.333	0.354
3.012	0.727	0.149	0.202	0.256	0.269	0.276	0.283
3.510	0.723	0.146	0.200	0.251	0.264	0.271	0.264
4.007	0.723	0.149	0.197	0.252	0.265	0.271	0.262
5.007	0.723	0.145	0.194	0.252	0.266	0.271	0.260
6.029	0.722	0.138	0.190	0.253	0.267	0.272	0.260
6.997	0.722	0.135	0.188	0.255	0.269	0.273	0.259
7.997	0.721	0.134	0.188	0.253	0.268	0.272	0.258

Table 14. Internal Static Pressure Ratios With A/B Power, Short Flap, and $\delta_{v,p} = 0°$

$\phi = 0°$

	Internal static pressure ratio for x/L_f of—						
NPR	-0.025	0.145	0.285	0.430	0.570	0.715	0.860
1.503	0.584	0.300	0.421	0.527	0.569	0.601	0.627
2.006	0.585	0.291	0.303	0.294	0.325	0.453	0.470
2.501	0.585	0.292	0.304	0.293	0.278	0.256	0.241
2.999	0.586	0.294	0.304	0.291	0.277	0.256	0.240
3.508	0.586	0.294	0.304	0.291	0.277	0.256	0.240
4.005	0.587	0.292	0.302	0.289	0.276	0.256	0.239
4.993	0.587	0.291	0.301	0.288	0.275	0.255	0.239
5.369	0.587	0.291	0.301	0.288	0.275	0.255	0.238

$\phi = 45°$

	Internal static pressure ratio for x/L_f of—			
NPR	0.200	0.400	0.600	0.800
1.503	0.307	0.490	0.570	0.617
2.006	0.302	0.297	0.349	0.463
2.501	0.304	0.296	0.270	0.242
2.999	0.304	0.295	0.270	0.242
3.508	0.303	0.294	0.269	0.242
4.005	0.303	0.295	0.269	0.242
4.993	0.302	0.295	0.269	0.242
5.369	0.302	0.295	0.269	0.241

$\phi = 90°$

	Internal static pressure ratio for x/L_f of—						
NPR	-0.025	0.145	0.285	0.430	0.570	0.715	0.860
1.503	0.581	0.299	0.408	0.517	0.564	0.598	0.628
2.006	0.582	0.294	0.302	0.297	0.311	0.455	0.472
2.501	0.581	0.296	0.302	0.296	0.282	0.260	0.242
2.999	0.582	0.297	0.302	0.295	0.281	0.260	0.240
3.508	0.582	0.297	0.301	0.294	0.281	0.260	0.240
4.005	0.582	0.297	0.300	0.294	0.280	0.259	0.240
4.993	0.582	0.296	0.299	0.294	0.280	0.260	0.240
5.369	0.582	0.296	0.299	0.294	0.280	0.260	0.239

Table 14. Concluded

$\phi = 135°$

	Internal static pressure ratio for x/L_f of—				
NPR	0.165	0.330	0.500	0.670	0.835
1.503	0.309	0.448	0.556	0.598	0.630
2.006	0.300	0.307	0.290	0.451	0.472
2.501	0.304	0.308	0.289	0.264	0.237
2.999	0.306	0.308	0.287	0.264	0.237
3.508	0.307	0.307	0.287	0.263	0.236
4.005	0.307	0.307	0.286	0.263	0.235
4.993	0.306	0.307	0.285	0.262	0.234
5.369	0.306	0.307	0.285	0.262	0.234

$\phi = 180°$

	Internal static pressure ratio for x/L_f of—						
NPR	-0.025	0.145	0.285	0.430	0.570	0.715	0.860
1.503	0.585	0.302	0.434	0.523	0.567	0.599	0.630
2.006	0.587	0.286	0.294	0.293	0.298	0.459	0.477
2.501	0.589	0.287	0.295	0.289	0.271	0.258	0.240
2.999	0.589	0.287	0.295	0.288	0.270	0.258	0.239
3.508	0.590	0.287	0.295	0.288	0.269	0.258	0.239
4.005	0.591	0.289	0.294	0.288	0.269	0.258	0.239
4.993	0.591	0.289	0.294	0.288	0.268	0.257	0.238
5.369	0.591	0.288	0.294	0.288	0.268	0.257	0.238

Table 15. Internal Static Pressure Ratios With A/B Power, Short Flap, and $\delta_{v,p} = 10°$

$\phi = 0°$

	Internal static pressure ratio for x/L_f of—						
NPR	-0.025	0.145	0.285	0.430	0.570	0.715	0.860
1.499	0.561	0.606	0.613	0.610	0.622	0.639	0.642
2.003	0.517	0.537	0.513	0.461	0.419	0.398	0.347
2.503	0.516	0.537	0.513	0.460	0.419	0.386	0.346
2.994	0.516	0.536	0.513	0.459	0.418	0.378	0.345
3.501	0.516	0.536	0.513	0.458	0.418	0.373	0.344
4.011	0.515	0.536	0.513	0.458	0.418	0.370	0.343
4.987	0.512	0.536	0.513	0.458	0.418	0.367	0.342
5.317	0.512	0.536	0.513	0.458	0.418	0.366	0.341

$\phi = 45°$

	Internal static pressure ratio for x/L_f of—			
NPR	0.200	0.400	0.600	0.800
1.499	0.591	0.610	0.627	0.640
2.003	0.476	0.451	0.383	0.331
2.503	0.476	0.451	0.382	0.331
2.994	0.476	0.450	0.382	0.331
3.501	0.475	0.449	0.381	0.331
4.011	0.475	0.449	0.381	0.331
4.987	0.477	0.449	0.380	0.330
5.317	0.477	0.449	0.380	0.330

$\phi = 90°$

	Internal static pressure ratio for x/L_f of—						
NPR	-0.025	0.145	0.285	0.430	0.570	0.715	0.860
1.499	0.532	0.521	0.582	0.604	0.623	0.636	0.649
2.003	0.526	0.291	0.312	0.329	0.419	0.461	0.469
2.503	0.525	0.295	0.312	0.327	0.321	0.291	0.265
2.994	0.525	0.295	0.310	0.326	0.320	0.290	0.265
3.501	0.525	0.293	0.309	0.326	0.319	0.290	0.264
4.011	0.525	0.293	0.309	0.326	0.319	0.289	0.264
4.987	0.525	0.291	0.305	0.329	0.320	0.289	0.264
5.317	0.526	0.291	0.305	0.329	0.320	0.289	0.263

Table 15. Concluded

$\phi = 135°$

	Internal static pressure ratio for x/L_f of—				
NPR	0.165	0.330	0.500	0.670	0.835
1.499	0.539	0.566	0.592	0.613	0.631
2.003	0.263	0.349	0.456	0.471	0.456
2.503	0.194	0.209	0.311	0.354	0.364
2.994	0.195	0.209	0.198	0.192	0.306
3.501	0.197	0.209	0.197	0.181	0.165
4.011	0.196	0.208	0.196	0.180	0.164
4.987	0.196	0.208	0.195	0.179	0.162
5.317	0.196	0.208	0.195	0.179	0.162

$\phi = 180°$

	Internal static pressure ratio for x/L_f of—						
NPR	-0.025	0.145	0.285	0.430	0.570	0.715	0.860
1.499	0.566	0.579	0.585	0.593	0.604	0.616	0.629
2.003	0.549	0.452	0.452	0.455	0.457	0.457	0.448
2.503	0.551	0.169	0.174	0.314	0.334	0.353	0.371
2.994	0.552	0.169	0.174	0.166	0.299	0.307	0.315
3.501	0.552	0.170	0.174	0.166	0.152	0.142	0.268
4.011	0.553	0.172	0.175	0.166	0.152	0.140	0.134
4.987	0.554	0.174	0.174	0.166	0.151	0.140	0.133
5.317	0.554	0.174	0.174	0.166	0.151	0.140	0.133

Table 16. Internal Static Pressure Ratios With A/B Power, Short Flap, and $\delta_{v,p} = 20°$

$\phi = 0°$

	Internal static pressure ratio for x/L_f of—						
NPR	-0.025	0.145	0.285	0.430	0.570	0.715	0.860
1.501	0.806	0.780	0.749	0.722	0.701	0.686	0.669
2.001	0.761	0.722	0.671	0.622	0.581	0.553	0.521
2.500	0.752	0.709	0.650	0.589	0.531	0.483	0.442
2.998	0.753	0.709	0.651	0.589	0.531	0.483	0.441
3.506	0.753	0.709	0.651	0.589	0.530	0.482	0.440
3.999	0.753	0.710	0.651	0.589	0.530	0.482	0.439
4.990	0.753	0.710	0.651	0.589	0.530	0.482	0.439
5.452	0.753	0.711	0.651	0.589	0.531	0.482	0.439

$\phi = 45°$

	Internal static pressure ratio for x/L_f of—			
NPR	0.200	0.400	0.600	0.800
1.501	0.734	0.710	0.688	0.668
2.001	0.648	0.599	0.552	0.512
2.500	0.627	0.551	0.474	0.408
2.998	0.627	0.551	0.474	0.407
3.506	0.627	0.550	0.473	0.407
3.999	0.627	0.550	0.472	0.406
4.990	0.627	0.551	0.472	0.406
5.452	0.627	0.551	0.472	0.406

$\phi = 90°$

	Internal static pressure ratio for x/L_f of—						
NPR	-0.025	0.145	0.285	0.430	0.570	0.715	0.860
1.501	0.606	0.651	0.670	0.669	0.665	0.661	0.656
2.001	0.555	0.513	0.547	0.523	0.509	0.497	0.484
2.500	0.551	0.395	0.422	0.441	0.473	0.433	0.391
2.998	0.551	0.395	0.422	0.393	0.357	0.346	0.371
3.506	0.551	0.394	0.421	0.392	0.356	0.323	0.291
3.999	0.552	0.393	0.420	0.392	0.356	0.323	0.291
4.990	0.553	0.392	0.421	0.392	0.355	0.323	0.290
5.452	0.553	0.391	0.421	0.392	0.356	0.323	0.290

Table 16. Concluded

$\phi = 135°$

NPR	Internal static pressure ratio for x/L_f of—				
	0.165	0.330	0.500	0.670	0.835
1.501	0.625	0.632	0.634	0.635	0.640
2.001	0.444	0.464	0.473	0.471	0.473
2.500	0.309	0.375	0.366	0.362	0.361
2.998	0.163	0.281	0.308	0.321	0.308
3.506	0.152	0.154	0.232	0.288	0.270
3.999	0.152	0.153	0.143	0.189	0.216
4.990	0.152	0.153	0.142	0.187	0.187
5.452	0.152	0.153	0.142	0.187	0.187

$\phi = 180°$

NPR	Internal static pressure ratio for x/L_f of—						
	-0.025	0.145	0.285	0.430	0.570	0.715	0.860
1.501	0.639	0.650	0.647	0.649	0.650	0.651	0.645
2.001	0.542	0.488	0.485	0.486	0.486	0.486	0.477
2.500	0.538	0.379	0.377	0.377	0.376	0.372	0.363
2.998	0.538	0.307	0.306	0.305	0.305	0.306	0.301
3.506	0.538	0.192	0.223	0.232	0.238	0.244	0.251
3.999	0.539	0.107	0.105	0.111	0.200	0.212	0.225
4.990	0.539	0.108	0.105	0.100	0.095	0.143	0.185
5.452	0.539	0.108	0.106	0.100	0.095	0.087	0.124

Table 17. Internal Static Pressure Ratios With A/B Power, Short Flap, and $\delta_{v,p} = 30°$

$\phi = 0°$

NPR	Internal static pressure ratio for x/L_f of—						
	-0.025	0.145	0.285	0.430	0.570	0.715	0.860
1.501	0.902	0.871	0.833	0.804	0.774	0.748	0.713
2.003	0.878	0.835	0.784	0.741	0.700	0.658	0.603
2.507	0.871	0.825	0.769	0.721	0.675	0.628	0.570
3.000	0.869	0.821	0.764	0.713	0.663	0.612	0.548
3.508	0.869	0.820	0.762	0.711	0.659	0.605	0.537
4.006	0.869	0.820	0.762	0.711	0.660	0.605	0.536
5.008	0.870	0.820	0.761	0.712	0.660	0.605	0.536
5.694	0.870	0.820	0.761	0.712	0.660	0.605	0.536

$\phi = 45°$

NPR	Internal static pressure ratio for x/L_f of—			
	0.200	0.400	0.600	0.800
1.501	0.817	0.777	0.742	0.704
2.003	0.760	0.700	0.643	0.582
2.507	0.743	0.672	0.606	0.536
3.000	0.735	0.659	0.587	0.513
3.508	0.733	0.654	0.574	0.490
4.006	0.733	0.654	0.574	0.488
5.008	0.733	0.655	0.574	0.487
5.694	0.733	0.655	0.574	0.487

$\phi = 90°$

NPR	Internal static pressure ratio for x/L_f of—						
	-0.025	0.145	0.285	0.430	0.570	0.715	0.860
1.501	0.696	0.712	0.710	0.697	0.682	0.675	0.664
2.003	0.618	0.605	0.598	0.573	0.545	0.521	0.493
2.507	0.601	0.558	0.557	0.516	0.483	0.448	0.422
3.000	0.597	0.514	0.534	0.507	0.454	0.404	0.372
3.508	0.596	0.509	0.493	0.458	0.455	0.404	0.344
4.006	0.596	0.509	0.493	0.450	0.403	0.359	0.350
5.008	0.596	0.509	0.493	0.449	0.403	0.356	0.312
5.694	0.596	0.509	0.492	0.449	0.403	0.356	0.312

Table 17. Concluded

$\phi = 135°$

	Internal static pressure ratio for x/L_f of—				
NPR	0.165	0.330	0.500	0.670	0.835
1.501	0.637	0.640	0.639	0.640	0.643
2.003	0.472	0.472	0.469	0.467	0.468
2.507	0.372	0.373	0.368	0.363	0.365
3.000	0.309	0.311	0.308	0.303	0.304
3.508	0.254	0.242	0.243	0.250	0.261
4.006	0.116	0.203	0.248	0.218	0.239
5.008	0.100	0.108	0.171	0.176	0.254
5.694	0.101	0.108	0.169	0.171	0.230

$\phi = 180°$

	Internal static pressure ratio for x/L_f of—						
NPR	-0.025	0.145	0.285	0.430	0.570	0.715	0.860
1.501	0.697	0.659	0.654	0.654	0.654	0.654	0.648
2.003	0.606	0.491	0.487	0.486	0.486	0.484	0.477
2.507	0.595	0.387	0.383	0.380	0.379	0.378	0.373
3.000	0.595	0.319	0.316	0.314	0.312	0.311	0.308
3.508	0.596	0.273	0.267	0.260	0.257	0.255	0.248
4.006	0.596	0.225	0.219	0.215	0.213	0.213	0.213
5.008	0.597	0.060	0.073	0.150	0.151	0.154	0.168
5.694	0.597	0.059	0.065	0.063	0.133	0.132	0.139

Table 18. Internal Static Pressure Ratios With A/B Power, Long Flap, and $\delta_{v,p} = 0°$

$\phi = 0°$

	Internal static pressure ratio for x/L_f of—						
NPR	-0.025	0.145	0.285	0.430	0.570	0.715	0.860
1.498	0.569	0.343	0.335	0.467	0.539	0.587	0.629
2.000	0.570	0.344	0.335	0.316	0.280	0.440	0.462
2.497	0.571	0.344	0.335	0.315	0.280	0.251	0.275
3.000	0.572	0.344	0.334	0.314	0.279	0.251	0.220
3.500	0.573	0.342	0.333	0.314	0.279	0.250	0.220
4.003	0.575	0.339	0.331	0.315	0.280	0.252	0.221
5.013	0.575	0.339	0.330	0.314	0.280	0.252	0.220
5.587	0.576	0.338	0.330	0.314	0.281	0.252	0.220

$\phi = 45°$

	Internal static pressure ratio for x/L_f of—			
NPR	0.200	0.400	0.600	0.800
1.498	0.329	0.408	0.553	0.618
2.000	0.328	0.323	0.275	0.453
2.497	0.328	0.322	0.274	0.231
3.000	0.327	0.321	0.273	0.231
3.500	0.326	0.321	0.272	0.231
4.003	0.329	0.321	0.272	0.231
5.013	0.329	0.321	0.272	0.231
5.587	0.329	0.321	0.272	0.230

$\phi = 90°$

	Internal static pressure ratio for x/L_f of—						
NPR	-0.025	0.145	0.285	0.430	0.570	0.715	0.860
1.498	0.570	0.345	0.343	0.510	0.556	0.593	0.629
2.000	0.572	0.346	0.338	0.313	0.283	0.444	0.465
2.497	0.572	0.347	0.338	0.313	0.282	0.249	0.302
3.000	0.573	0.346	0.337	0.313	0.281	0.249	0.218
3.500	0.573	0.345	0.336	0.313	0.281	0.249	0.218
4.003	0.575	0.343	0.336	0.314	0.282	0.249	0.218
5.013	0.576	0.342	0.335	0.315	0.282	0.249	0.218
5.587	0.576	0.342	0.335	0.315	0.282	0.249	0.218

Table 18. Concluded

$\phi = 135°$

NPR	Internal static pressure ratio for x/L_f of—				
	0.165	0.330	0.500	0.670	0.835
1.498	0.354	0.467	0.552	0.580	0.616
2.000	0.355	0.336	0.296	0.432	0.466
2.497	0.356	0.337	0.295	0.259	0.230
3.000	0.355	0.337	0.294	0.259	0.224
3.500	0.355	0.337	0.293	0.258	0.224
4.003	0.355	0.337	0.291	0.258	0.224
5.013	0.355	0.337	0.291	0.257	0.224
5.587	0.355	0.336	0.290	0.257	0.224

$\phi = 180°$

NPR	Internal static pressure ratio for x/L_f of—						
	-0.025	0.145	0.285	0.430	0.570	0.715	0.860
1.498	0.575	0.328	0.361	0.530	0.564	0.627	0.597
2.000	0.575	0.331	0.340	0.315	0.285	0.470	0.452
2.497	0.577	0.329	0.336	0.316	0.286	0.289	0.248
3.000	0.577	0.329	0.335	0.316	0.285	0.211	0.247
3.500	0.578	0.329	0.335	0.316	0.285	0.211	0.247
4.003	0.579	0.329	0.336	0.316	0.285	0.209	0.246
5.013	0.579	0.329	0.336	0.316	0.285	0.209	0.245
5.587	0.578	0.328	0.336	0.317	0.285	0.208	0.245

Table 19. Internal Static Pressure Ratios With A/B Power, Long Flap, and $\delta_{v,p} = 10°$

$\phi = 0°$

	Internal static pressure ratio for x/L_f of—						
NPR	-0.025	0.145	0.285	0.430	0.570	0.715	0.860
1.501	0.596	0.623	0.588	0.586	0.613	0.630	0.646
2.010	0.569	0.583	0.506	0.443	0.381	0.323	0.328
2.503	0.569	0.585	0.505	0.441	0.380	0.323	0.283
3.011	0.569	0.585	0.505	0.439	0.379	0.322	0.283
3.508	0.569	0.585	0.505	0.439	0.379	0.322	0.282
4.004	0.567	0.586	0.506	0.439	0.378	0.322	0.281
5.001	0.566	0.586	0.506	0.439	0.378	0.322	0.281
5.509	0.566	0.586	0.506	0.439	0.378	0.322	0.280

$\phi = 45°$

	Internal static pressure ratio for x/L_f of—			
NPR	0.200	0.400	0.600	0.800
1.501	0.591	0.589	0.620	0.641
2.010	0.520	0.433	0.353	0.285
2.503	0.519	0.432	0.352	0.281
3.011	0.519	0.431	0.351	0.281
3.508	0.519	0.430	0.351	0.281
4.004	0.519	0.430	0.350	0.281
5.001	0.519	0.429	0.350	0.281
5.509	0.519	0.429	0.350	0.281

$\phi = 90°$

	Internal static pressure ratio for x/L_f of—						
NPR	-0.025	0.145	0.285	0.430	0.570	0.715	0.860
1.501	0.557	0.567	0.581	0.595	0.613	0.630	0.645
2.010	0.553	0.419	0.405	0.356	0.357	0.376	0.468
2.503	0.553	0.418	0.404	0.351	0.311	0.269	0.234
3.011	0.553	0.418	0.404	0.350	0.310	0.269	0.233
3.508	0.553	0.418	0.404	0.350	0.310	0.269	0.233
4.004	0.554	0.420	0.405	0.351	0.310	0.268	0.233
5.001	0.554	0.420	0.406	0.351	0.309	0.268	0.232
5.509	0.554	0.420	0.406	0.351	0.309	0.268	0.232

Table 19. Concluded

$\phi = 135°$

NPR	Internal static pressure ratio for x/L_f of—				
	0.165	0.330	0.500	0.670	0.835
1.501	0.514	0.552	0.579	0.604	0.625
2.010	0.256	0.402	0.422	0.436	0.453
2.503	0.242	0.231	0.312	0.343	0.360
3.011	0.242	0.231	0.262	0.239	0.203
3.508	0.242	0.230	0.262	0.239	0.203
4.004	0.242	0.229	0.262	0.239	0.203
5.001	0.241	0.229	0.261	0.239	0.202
5.509	0.241	0.229	0.261	0.239	0.202

$\phi = 180°$

NPR	Internal static pressure ratio for x/L_f of—						
	-0.025	0.145	0.285	0.430	0.570	0.715	0.860
1.501	0.564	0.530	0.541	0.560	0.581	0.603	0.627
2.010	0.554	0.302	0.387	0.409	0.421	0.434	0.453
2.503	0.554	0.199	0.200	0.335	0.341	0.346	0.361
3.011	0.555	0.201	0.194	0.175	0.161	0.156	0.277
3.508	0.555	0.202	0.194	0.175	0.161	0.156	0.273
4.004	0.556	0.202	0.194	0.175	0.161	0.156	0.272
5.001	0.557	0.201	0.194	0.175	0.160	0.156	0.270
5.509	0.557	0.201	0.194	0.175	0.160	0.156	0.269

Table 20. Internal Static Pressure Ratios With A/B Power, Long Flap, and $\delta_{v,p} = 20°$

$\phi = 0°$

	Internal static pressure ratio for x/L_f of—						
NPR	-0.025	0.145	0.285	0.430	0.570	0.715	0.860
1.505	0.816	0.777	0.737	0.708	0.681	0.666	0.652
2.005	0.777	0.721	0.659	0.603	0.546	0.503	0.468
2.503	0.768	0.706	0.633	0.561	0.485	0.430	0.390
3.004	0.767	0.705	0.632	0.558	0.478	0.413	0.349
3.511	0.767	0.705	0.632	0.558	0.477	0.413	0.348
4.000	0.767	0.706	0.632	0.558	0.477	0.413	0.348
4.996	0.769	0.707	0.632	0.559	0.477	0.413	0.347
5.639	0.769	0.707	0.632	0.559	0.477	0.412	0.347

$\phi = 45°$

	Internal static pressure ratio for x/L_f of—			
NPR	0.200	0.400	0.600	0.800
1.505	0.737	0.696	0.667	0.656
2.005	0.661	0.584	0.514	0.474
2.503	0.634	0.527	0.451	0.391
3.004	0.633	0.523	0.423	0.340
3.511	0.633	0.522	0.422	0.340
4.000	0.633	0.522	0.421	0.339
4.996	0.633	0.522	0.421	0.339
5.639	0.633	0.523	0.421	0.339

$\phi = 90°$

	Internal static pressure ratio for x/L_f of—						
NPR	-0.025	0.145	0.285	0.430	0.570	0.715	0.860
1.505	0.650	0.674	0.662	0.655	0.647	0.643	0.643
2.005	0.594	0.577	0.533	0.509	0.485	0.465	0.456
2.503	0.587	0.495	0.488	0.452	0.403	0.362	0.367
3.004	0.587	0.495	0.432	0.390	0.335	0.284	0.245
3.511	0.587	0.495	0.431	0.389	0.334	0.283	0.244
4.000	0.588	0.495	0.430	0.389	0.334	0.283	0.243
4.996	0.590	0.496	0.430	0.389	0.334	0.283	0.243
5.639	0.590	0.496	0.429	0.389	0.334	0.283	0.243

Table 20. Concluded

$\phi = 135°$

NPR	Internal static pressure ratio for x/L_f of—				
	0.165	0.330	0.500	0.670	0.835
1.505	0.601	0.607	0.613	0.620	0.630
2.005	0.446	0.446	0.449	0.453	0.463
2.503	0.339	0.341	0.348	0.353	0.363
3.004	0.174	0.250	0.260	0.227	0.199
3.511	0.175	0.249	0.260	0.226	0.199
4.000	0.175	0.248	0.260	0.226	0.199
4.996	0.175	0.247	0.259	0.226	0.199
5.639	0.174	0.246	0.259	0.226	0.199

$\phi = 180°$

NPR	Internal static pressure ratio for x/L_f of—						
	-0.025	0.145	0.285	0.430	0.570	0.715	0.860
1.505	0.643	0.624	0.615	0.613	0.615	0.625	0.636
2.005	0.565	0.467	0.457	0.454	0.455	0.463	0.467
2.503	0.560	0.361	0.350	0.347	0.347	0.356	0.366
3.004	0.560	0.120	0.114	0.107	0.167	0.217	0.273
3.511	0.560	0.121	0.114	0.108	0.120	0.216	0.270
4.000	0.559	0.123	0.114	0.108	0.117	0.215	0.269
4.996	0.559	0.123	0.114	0.108	0.112	0.214	0.267
5.639	0.559	0.123	0.114	0.107	0.110	0.215	0.267

Table 21. Internal Static Pressure Ratios With A/B Power, Long Flap, and $\delta_{v,p} = 30°$

$\phi = 0°$

NPR	Internal static pressure ratio for x/L_f of—						
	-0.025	0.145	0.285	0.430	0.570	0.715	0.860
1.499	0.921	0.866	0.822	0.781	0.746	0.715	0.692
2.004	0.902	0.829	0.765	0.701	0.641	0.580	0.529
2.499	0.896	0.817	0.746	0.671	0.598	0.523	0.457
2.998	0.895	0.814	0.742	0.664	0.586	0.502	0.422
3.505	0.896	0.814	0.742	0.664	0.586	0.501	0.422
4.006	0.896	0.814	0.742	0.664	0.586	0.501	0.421
5.011	0.896	0.814	0.742	0.665	0.586	0.500	0.420
5.392	0.897	0.814	0.742	0.665	0.586	0.500	0.420

$\phi = 45°$

NPR	Internal static pressure ratio for x/L_f of—			
	0.200	0.400	0.600	0.800
1.499	0.810	0.756	0.709	0.682
2.004	0.749	0.661	0.573	0.510
2.499	0.728	0.622	0.511	0.436
2.998	0.723	0.609	0.483	0.389
3.505	0.722	0.609	0.481	0.389
4.006	0.722	0.609	0.480	0.389
5.011	0.722	0.610	0.479	0.389
5.392	0.722	0.610	0.479	0.388

$\phi = 90°$

NPR	Internal static pressure ratio for x/L_f of—						
	-0.025	0.145	0.285	0.430	0.570	0.715	0.860
1.499	0.724	0.728	0.711	0.689	0.670	0.656	0.654
2.004	0.646	0.629	0.591	0.546	0.506	0.475	0.461
2.499	0.626	0.579	0.539	0.479	0.428	0.384	0.363
2.998	0.622	0.563	0.506	0.434	0.367	0.305	0.263
3.505	0.621	0.562	0.505	0.434	0.367	0.305	0.263
4.006	0.621	0.562	0.505	0.433	0.367	0.304	0.262
5.011	0.620	0.562	0.504	0.433	0.366	0.304	0.262
5.392	0.620	0.562	0.504	0.433	0.366	0.304	0.261

Table 21. Concluded

$\phi = 135°$

Internal static pressure ratio for x/L_f of—

NPR	0.165	0.330	0.500	0.670	0.835
1.499	0.612	0.617	0.621	0.626	0.634
2.004	0.431	0.431	0.439	0.449	0.461
2.499	0.305	0.317	0.335	0.347	0.359
2.998	0.119	0.238	0.262	0.229	0.205
3.505	0.119	0.235	0.262	0.228	0.205
4.006	0.120	0.231	0.263	0.228	0.204
5.011	0.122	0.224	0.264	0.228	0.204
5.392	0.122	0.221	0.264	0.228	0.204

$\phi = 180°$

Internal static pressure ratio for x/L_f of—

NPR	-0.025	0.145	0.285	0.430	0.570	0.715	0.860
1.499	0.686	0.634	0.625	0.622	0.623	0.630	0.638
2.004	0.604	0.456	0.443	0.439	0.442	0.451	0.464
2.499	0.596	0.331	0.322	0.322	0.330	0.340	0.359
2.998	0.596	0.073	0.071	0.161	0.182	0.260	0.293
3.505	0.596	0.073	0.071	0.140	0.175	0.256	0.283
4.006	0.597	0.073	0.072	0.141	0.173	0.255	0.279
5.011	0.597	0.073	0.072	0.140	0.172	0.257	0.278
5.392	0.597	0.073	0.072	0.139	0.172	0.259	0.278

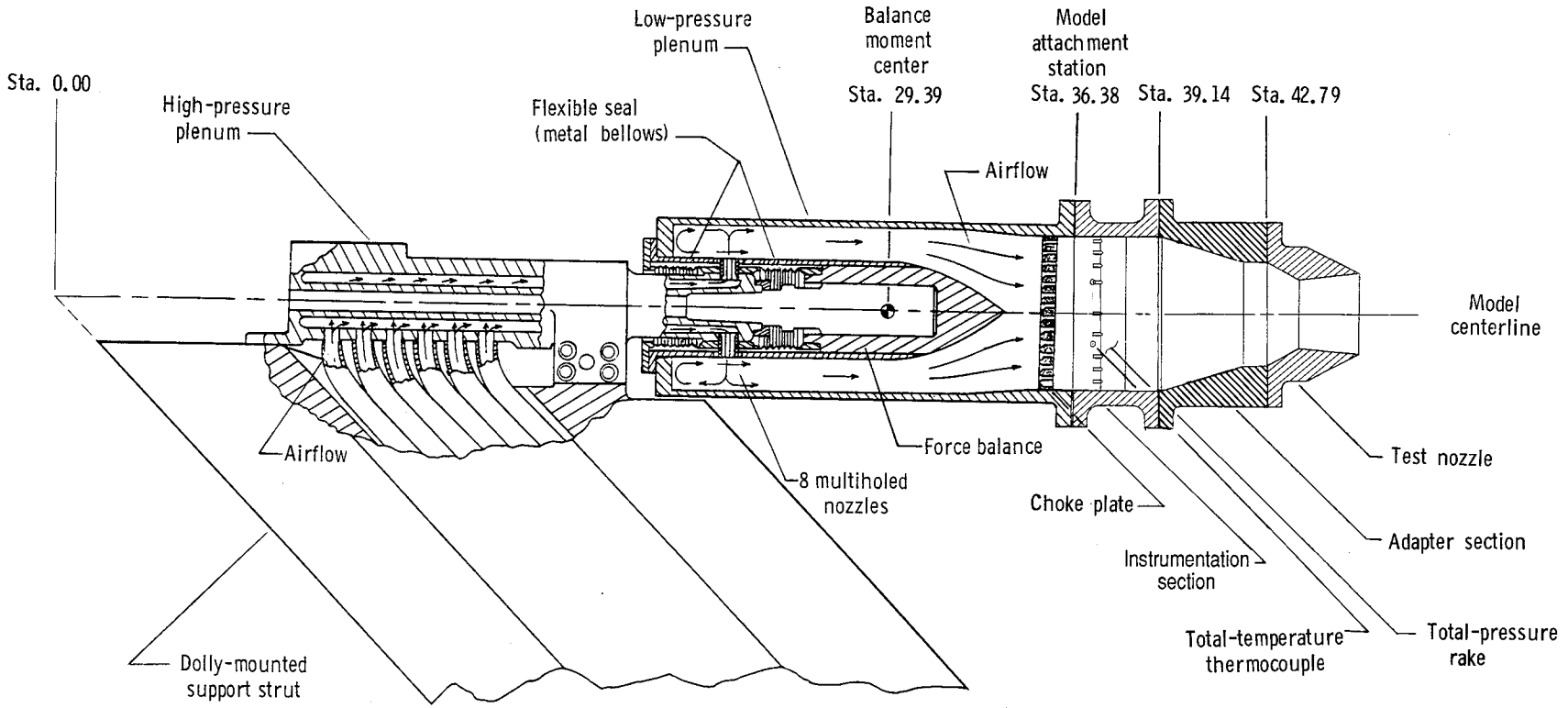

(a) Air-powered nacelle test apparatus.

Figure 1. Air-powered nacelle model with typical nozzle configuration installed. All linear dimensions are in inches.

L-88-13,169

(b) Test apparatus with dry power nozzle.

Figure 1. Concluded.

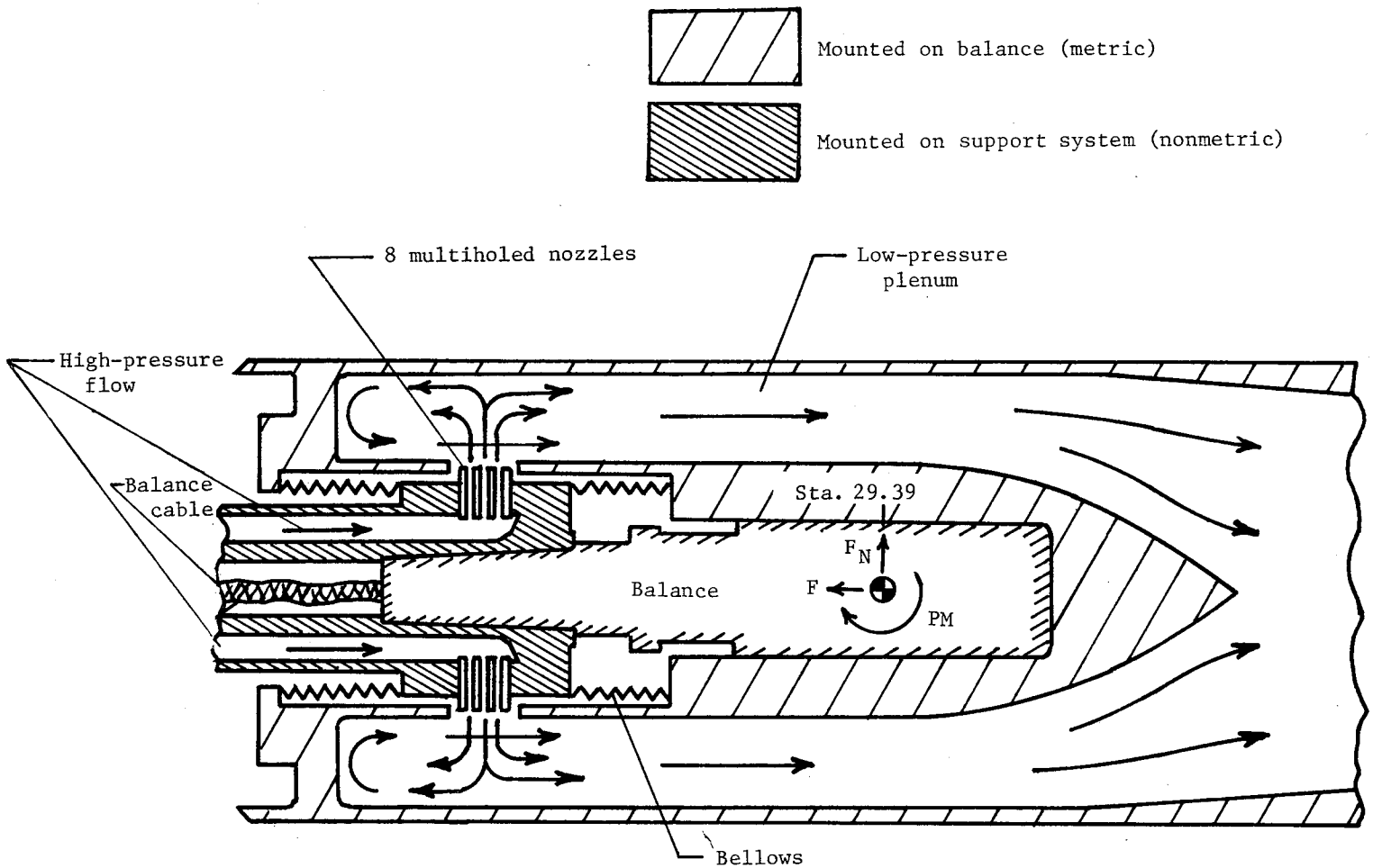

Figure 2. Schematic cross section of the high-pressure airflow transfer system.

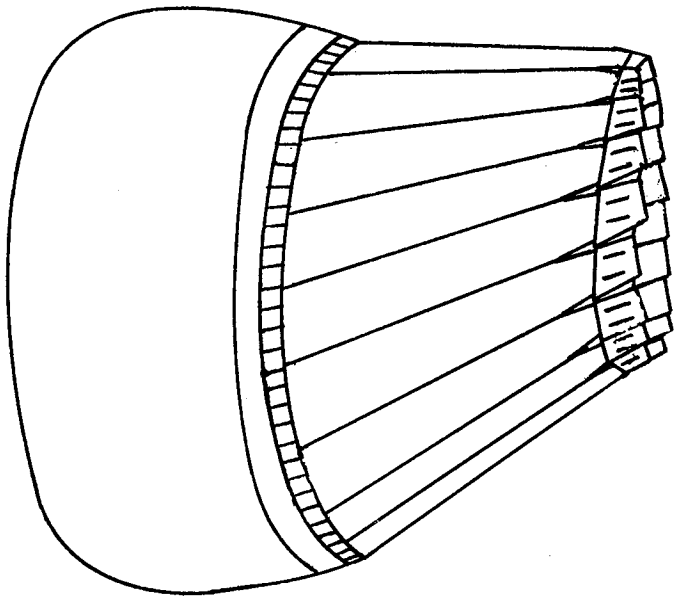

Figure 3. Pitch- and yaw-vectoring axisymmetric nozzle.

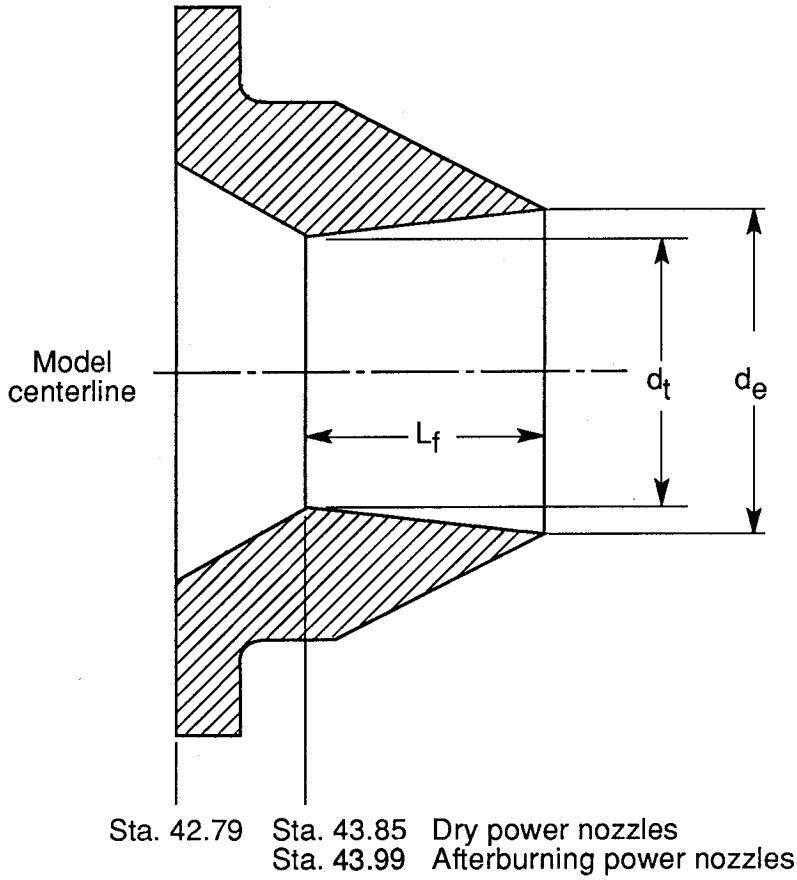

$[(NPR)_{des} = 5.01; \quad A_e/A_t = 1.35]$

Power setting	Flap	A_t, in^2	A_e, in^2	d_t, in^2	d_e, in^2	L_f, in	L_f/d_t
Dry	Short	4.03	5.44	2.266	2.633	1.992	0.88
Dry	Long	4.03	5.44	2.266	2.633	2.994	1.32
Afterburning	Short	7.49	10.11	3.088	3.088	1.984	.64
Afterburning	Long	7.49	10.11	3.088	3.088	2.990	.97

Figure 4. Geometry of unvectored nozzle. All linear dimensions are in inches.

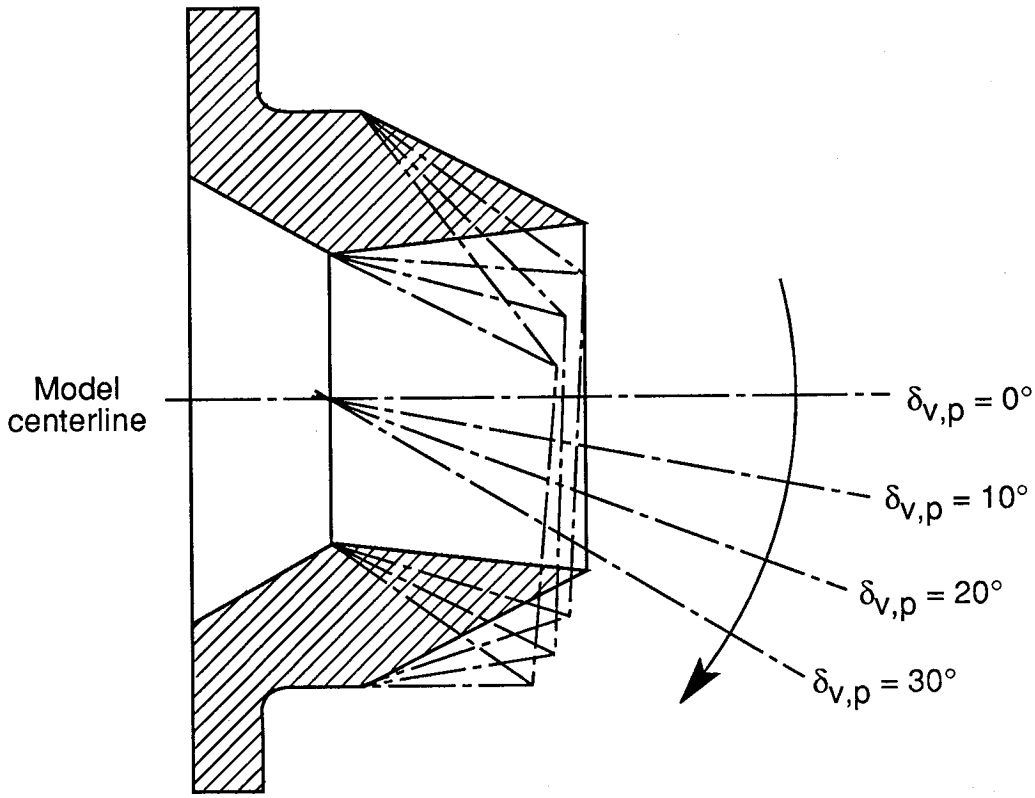

Figure 5. Vector angles of the vectored nozzle models.

L-88-13,170

(a) $\delta_{v,p} = 0°$.

Figure 6. Dry power nozzle. $L_f/d_t = 0.88$.

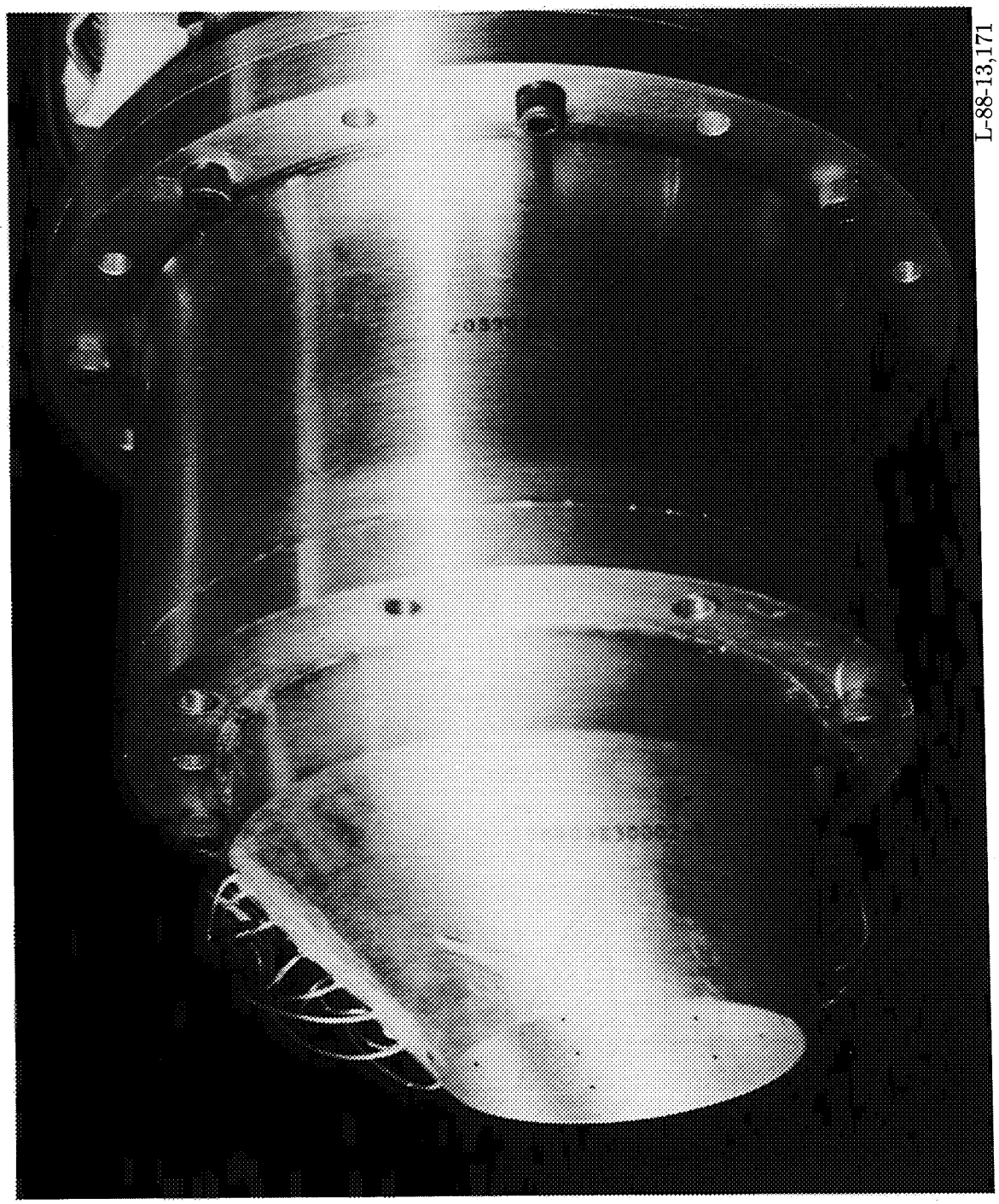

L-88-13,171

(b) $\delta_{v,p} = 20°$.

Figure 6. Concluded.

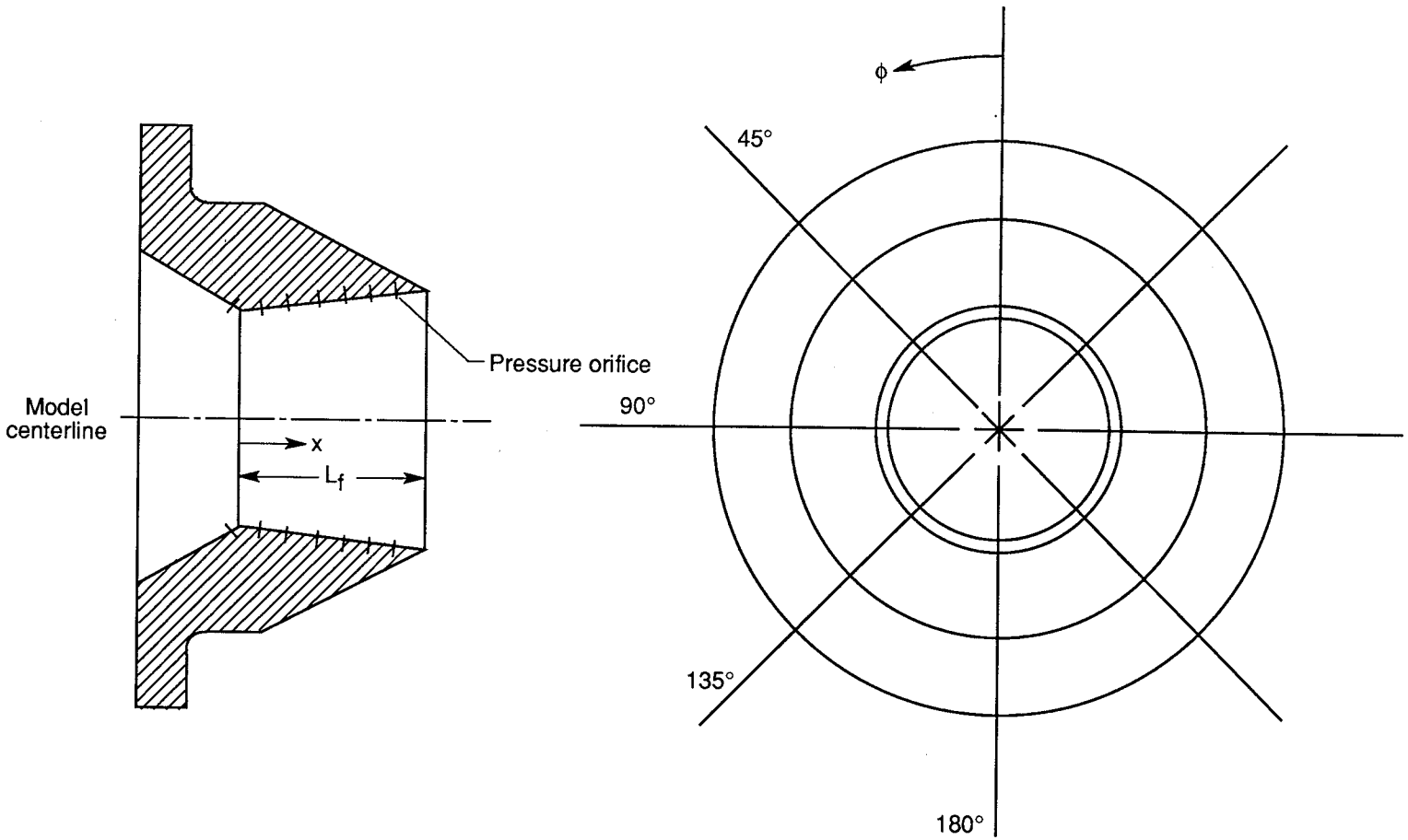

ϕ, deg	x/L_f															
	-0.025	0.145	0.165	0.200	0.285	0.330	0.400	0.430	0.500	0.570	0.600	0.670	0.715	0.800	0.835	0.860
0	✓	✓			✓			✓		✓			✓			✓
45				✓			✓				✓			✓		
90		✓			✓			✓		✓			✓			✓
135			✓			✓			✓			✓			✓	
180	✓	✓			✓			✓		✓			✓			✓

Figure 7. Internal pressure orifice locations (indicated in chart by checkmarks).

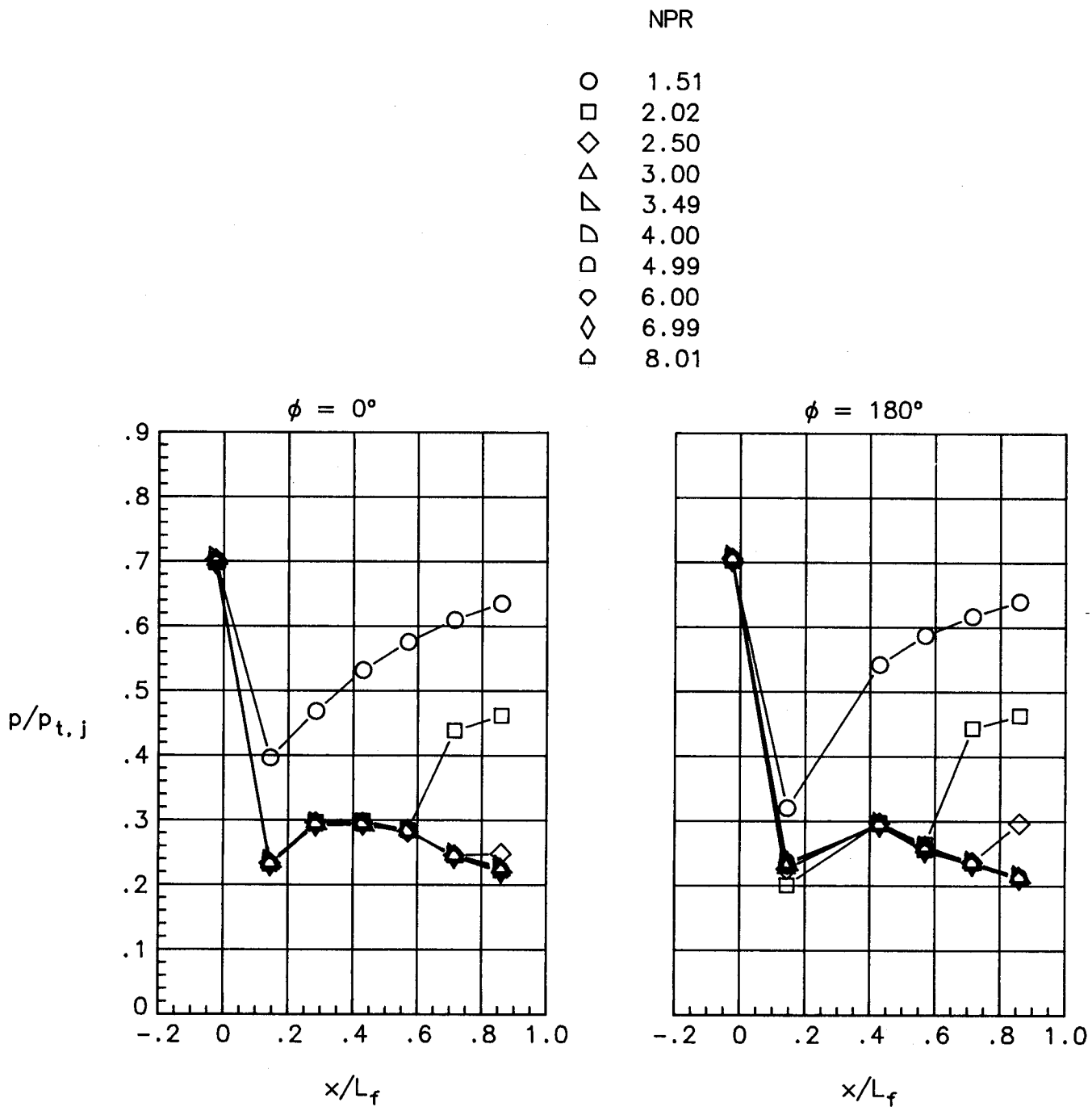

(a) $\delta_{v,p} = 0°$.

Figure 8. Pressure distributions. Dry power; $L_f/d_t = 0.88$.

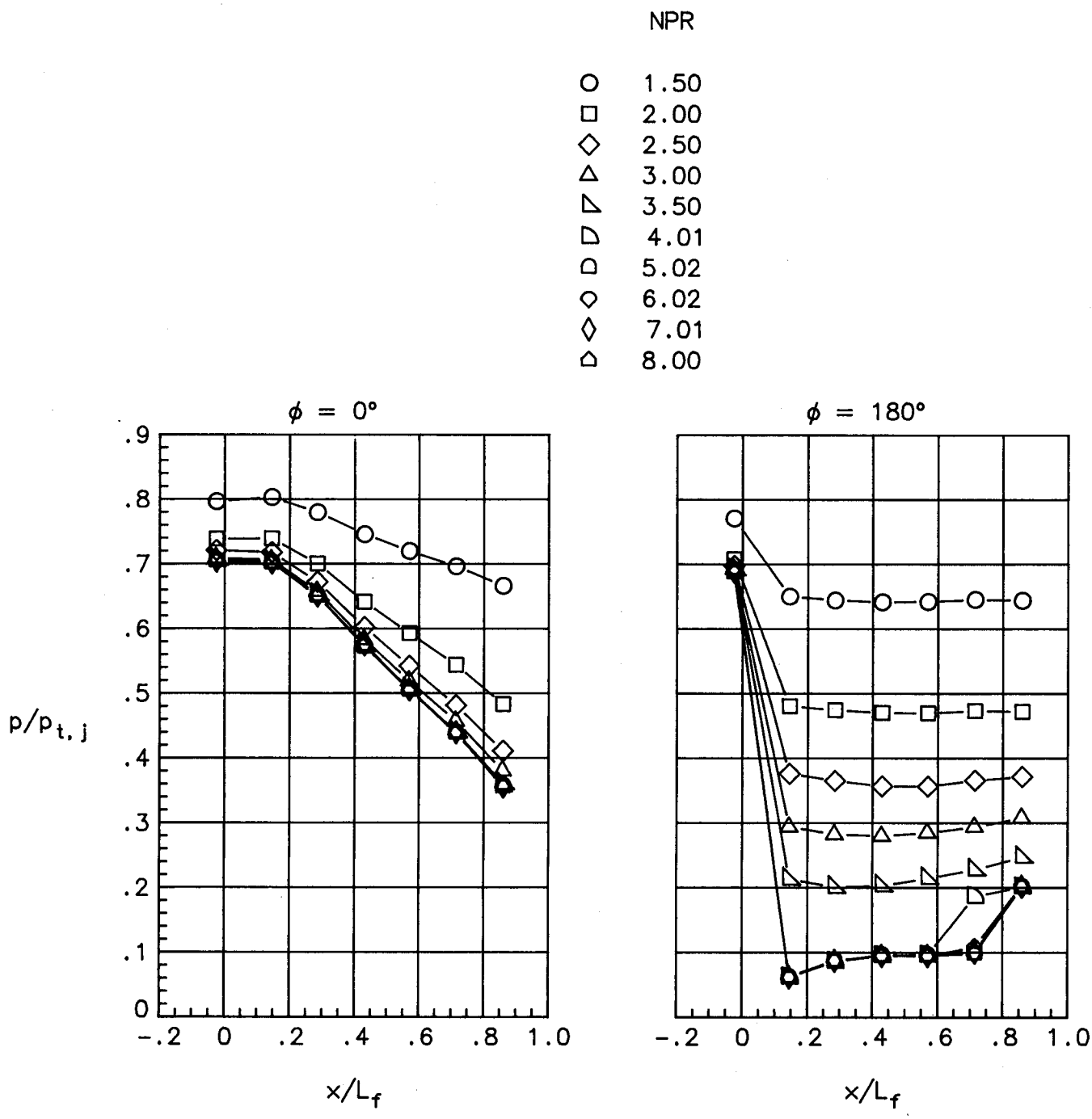

(b) $\delta_{v,p} = 20°$.

Figure 8. Concluded.

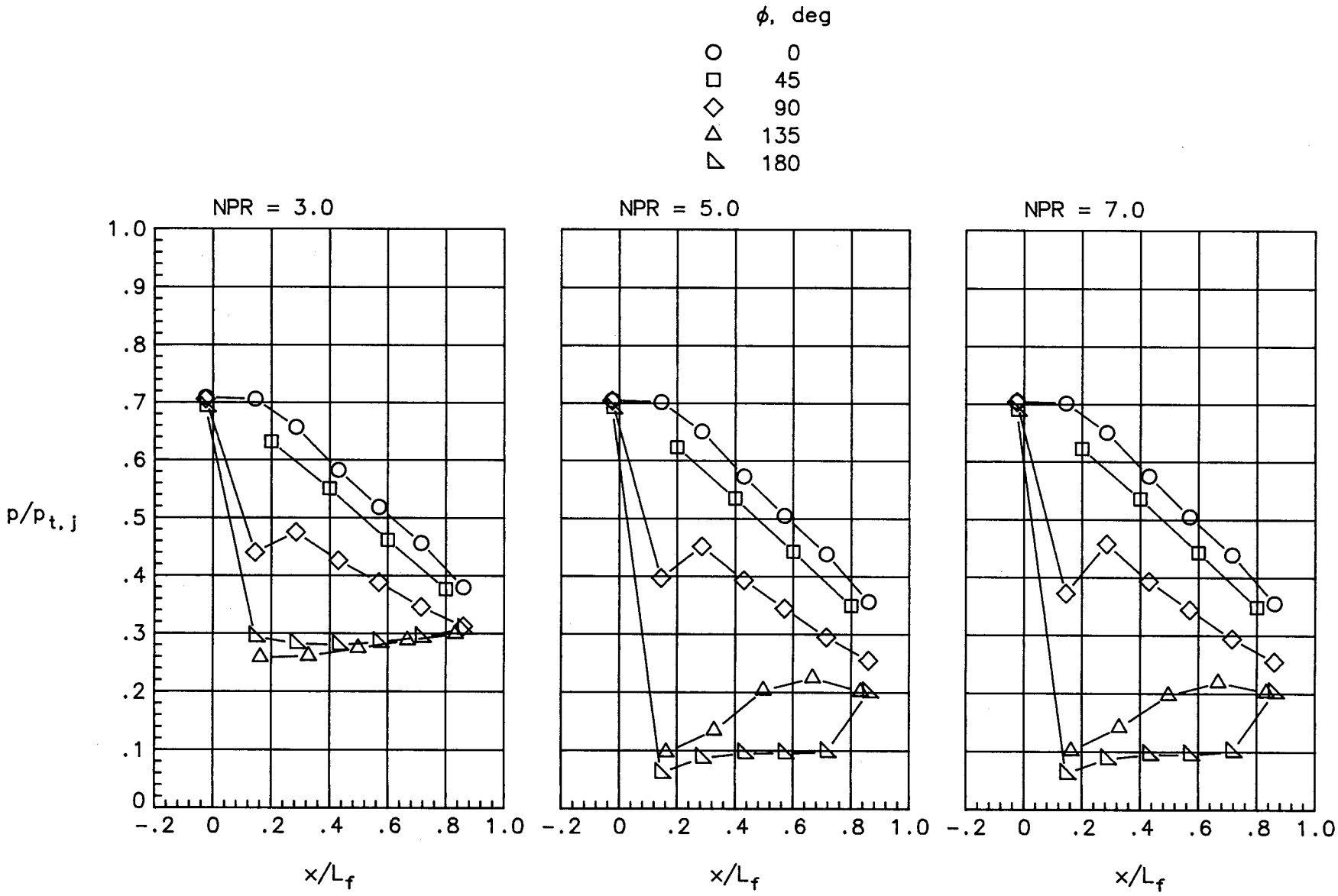

Figure 9. Pressure distributions. Dry power; $L_f/d_t = 0.88$; $\delta_{v,p} = 20°$.

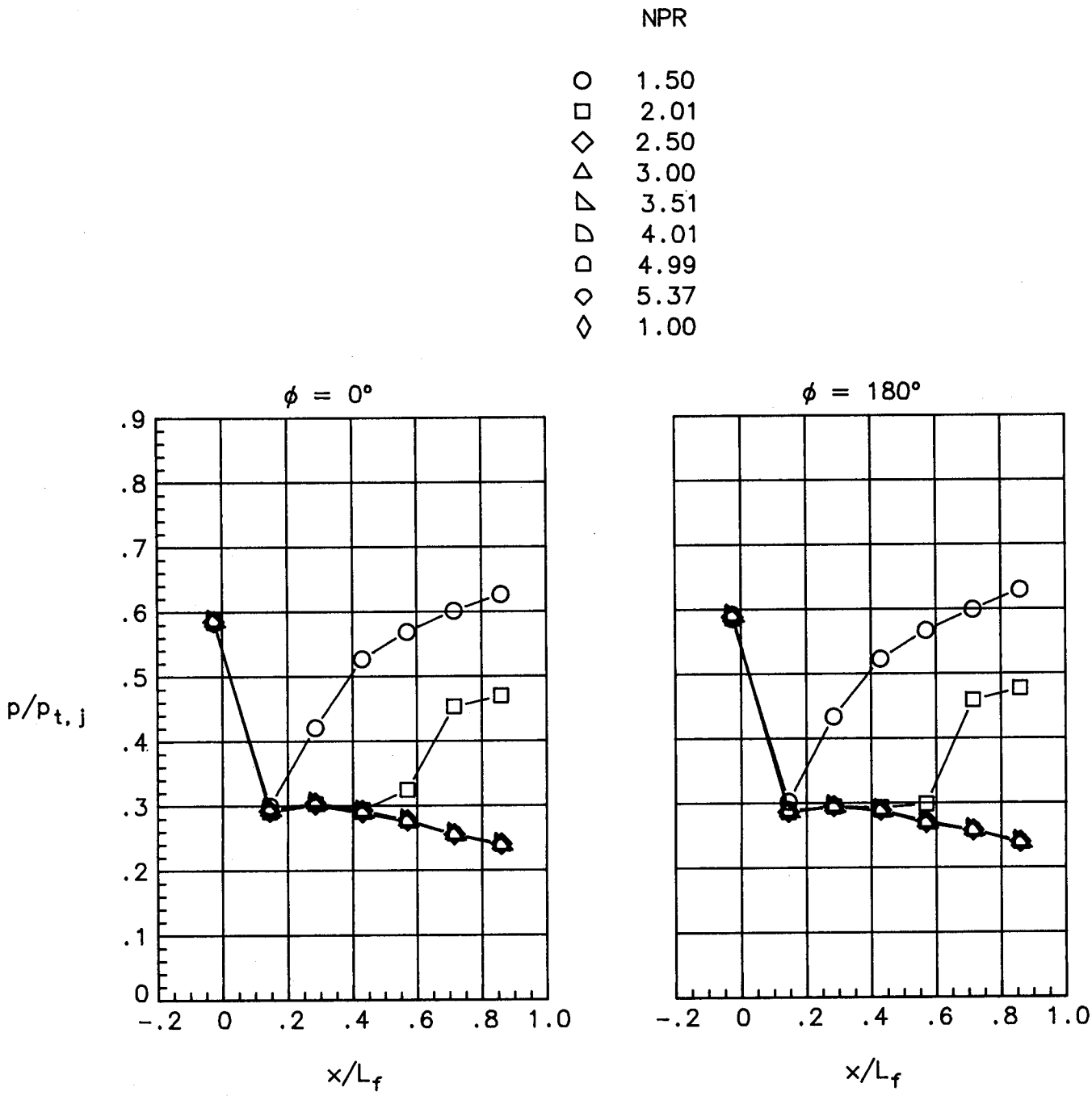

(a) $\delta_{v,p} = 0°$.

Figure 10. Pressure distributions. A/B power; $L_f/d_t = 0.64$.

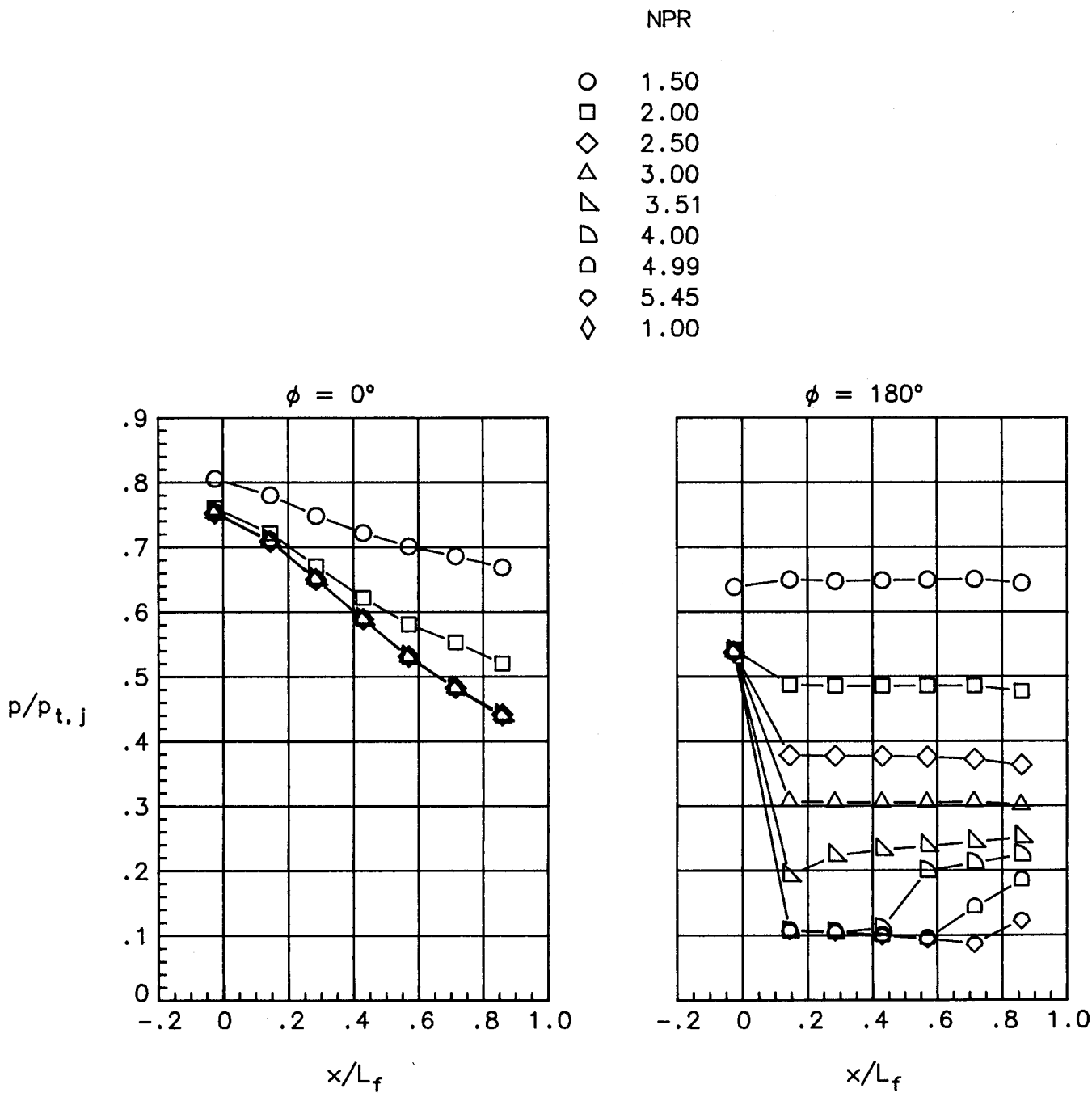

(b) $\delta_{v,p} = 20°$.

Figure 10. Concluded.

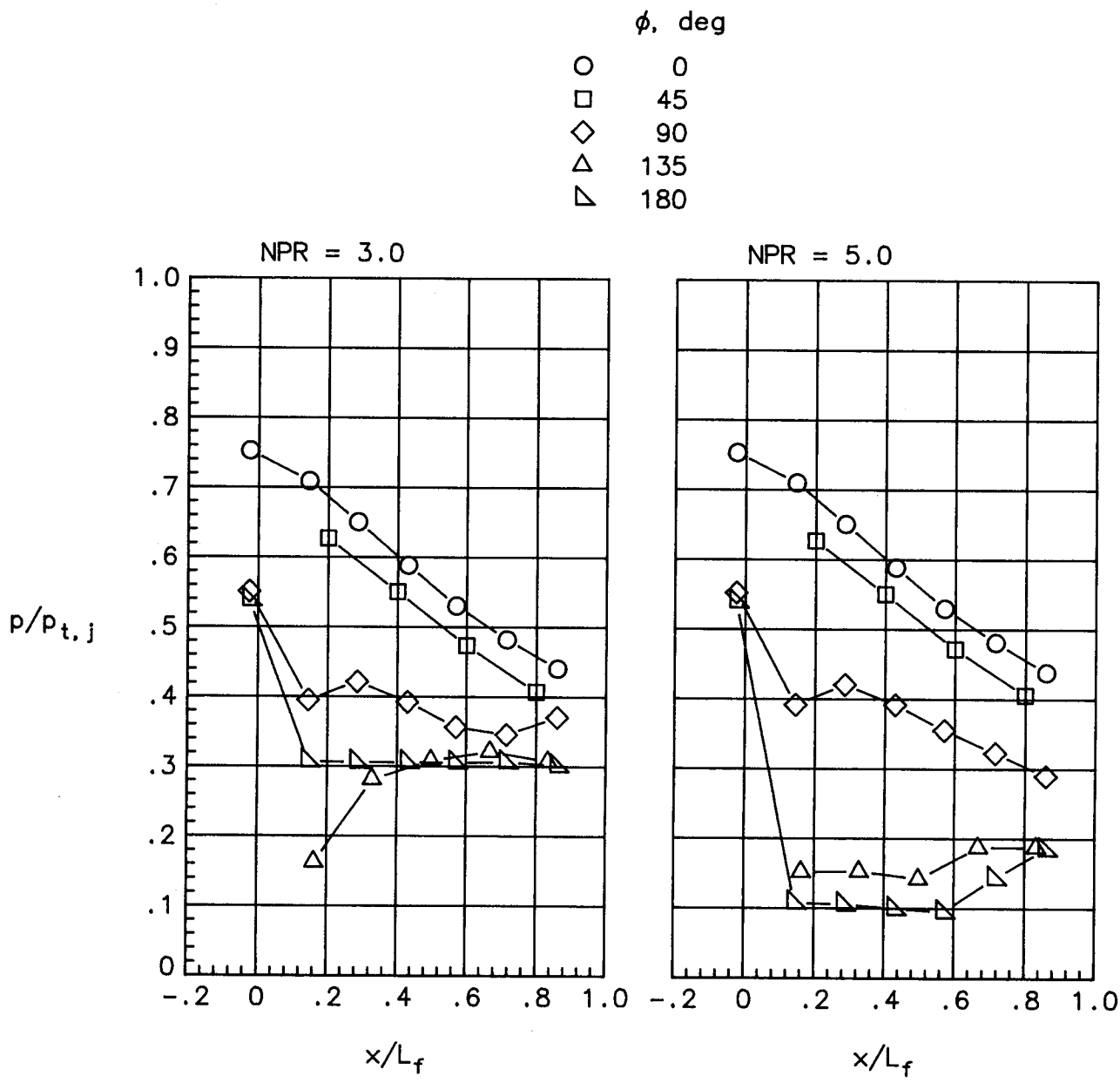

Figure 11. Pressure distributions. A/B power; $L_f/d_t = 0.64$; $\delta_{v,p} = 20°$.

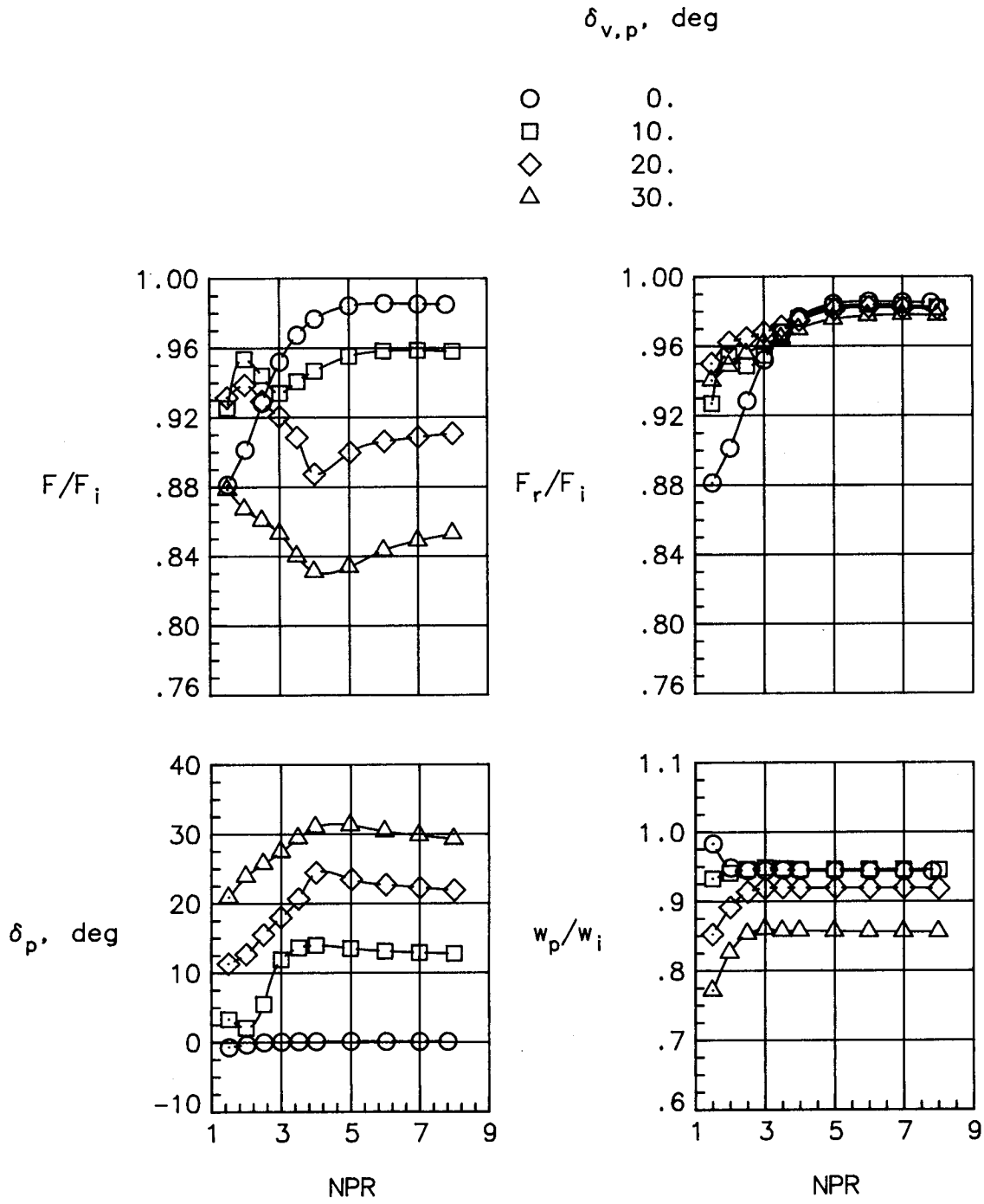

(a) Thrust and turning performance.

Figure 12. Effect of pitch vectoring on internal performance. Dry power; $L_f/d_t = 0.88$.

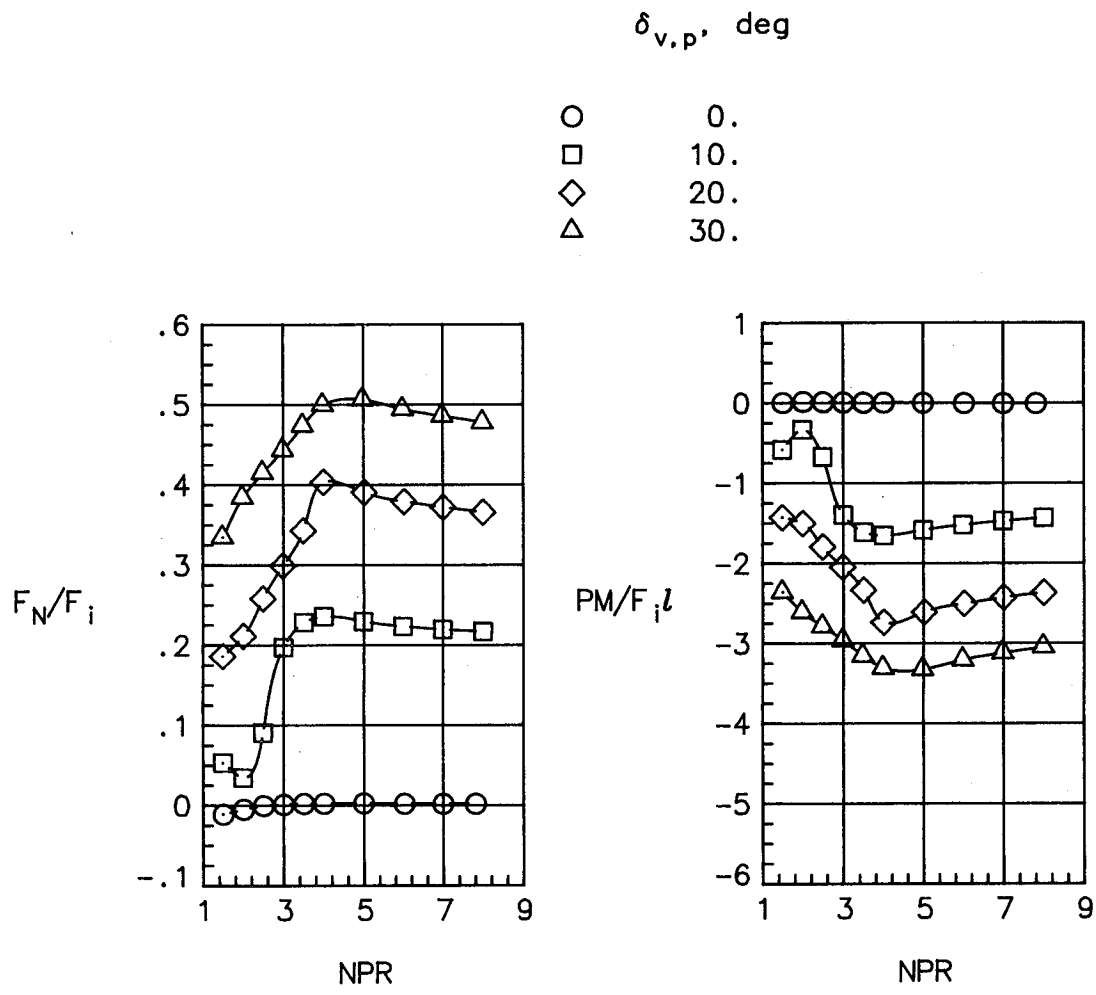

(b) Force and moment characteristics.

Figure 12. Concluded.

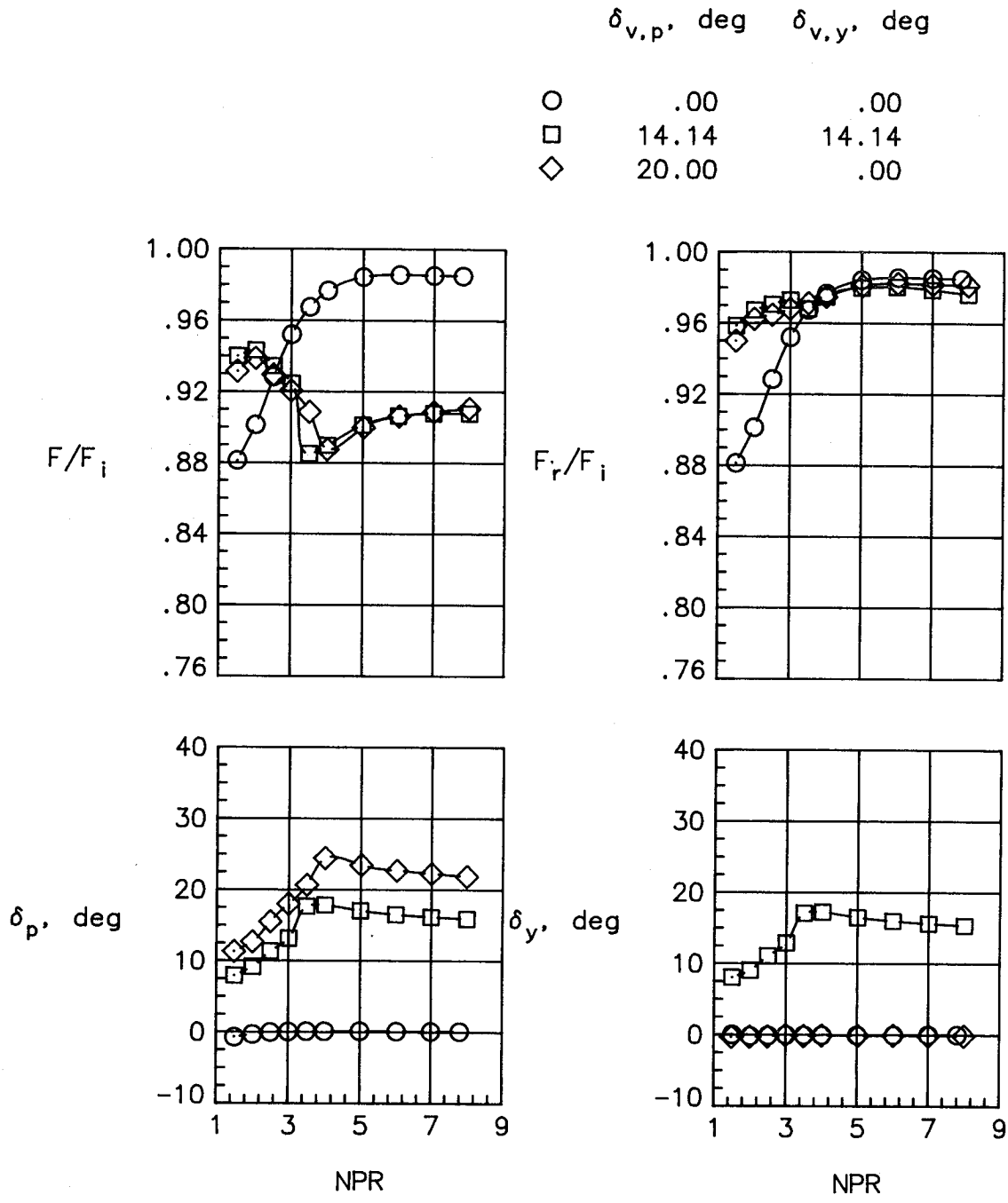

(a) Thrust and turning performance.

Figure 13. Effect of combined vectoring on internal performance. Dry power; $L_f/d_t = 0.88$.

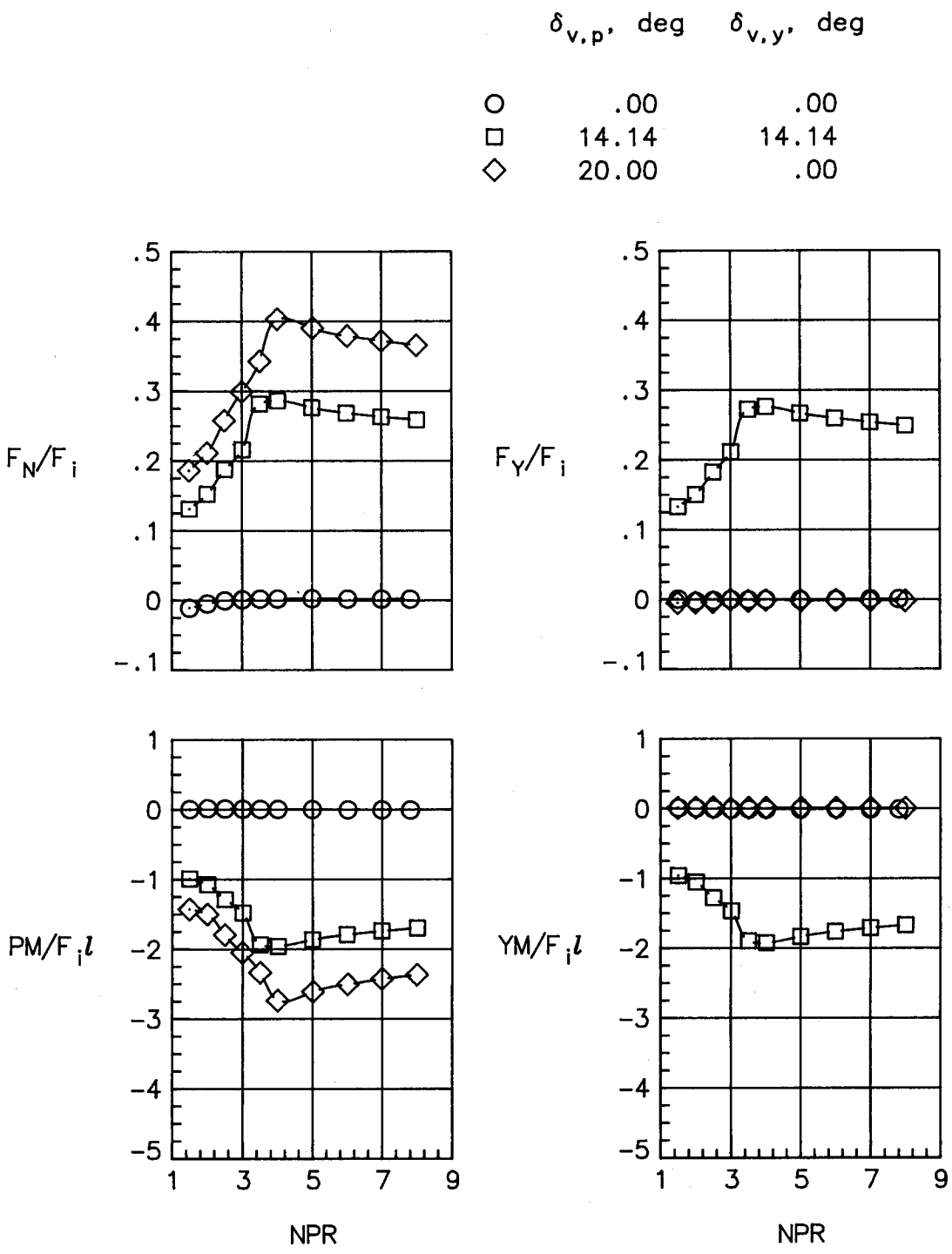

(b) Force and moment characteristics.

Figure 13. Concluded.

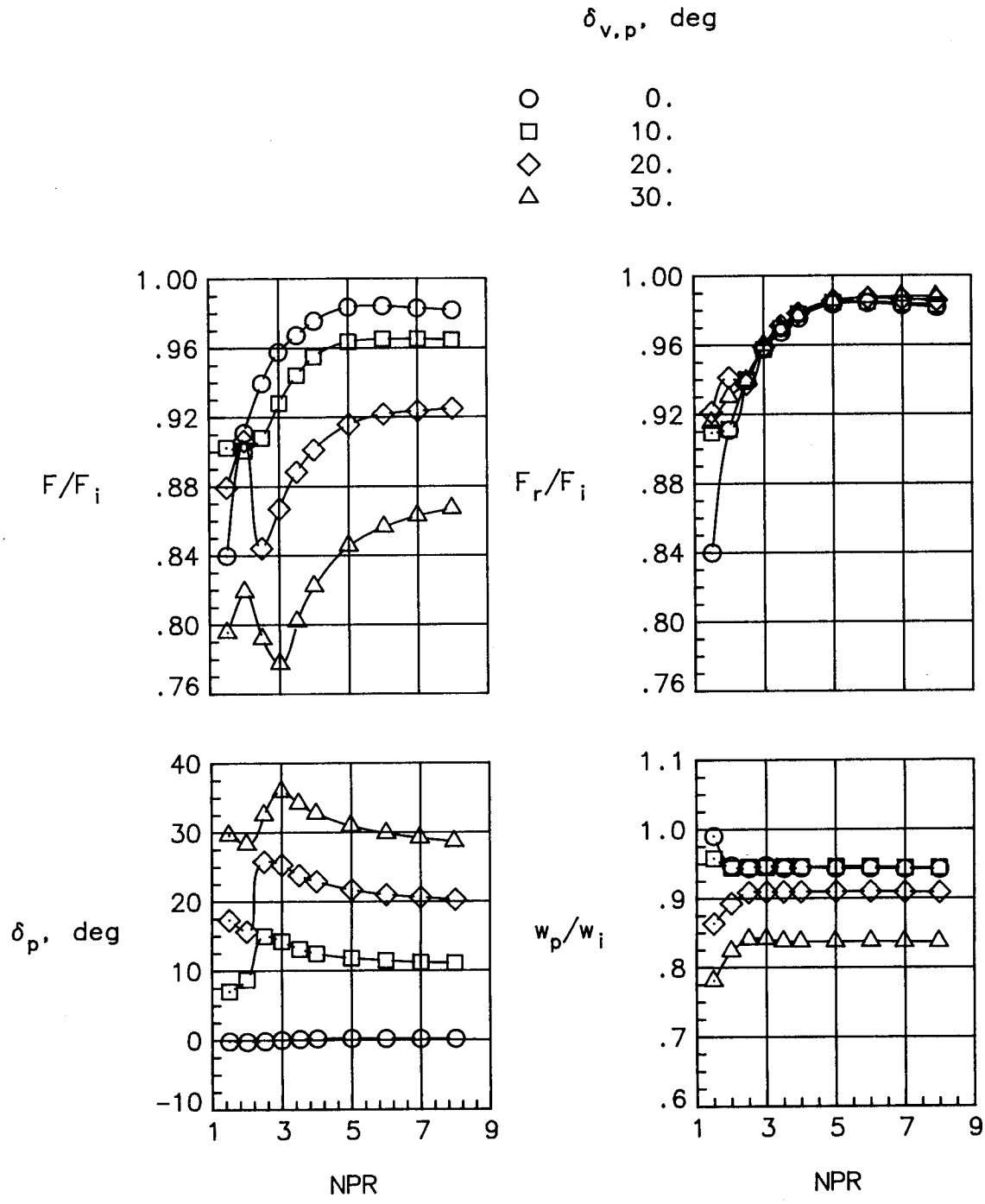

(a) Thrust and turning performance.

Figure 14. Effect of pitch vectoring on internal performance. Dry power; $L_f/d_t = 1.32$.

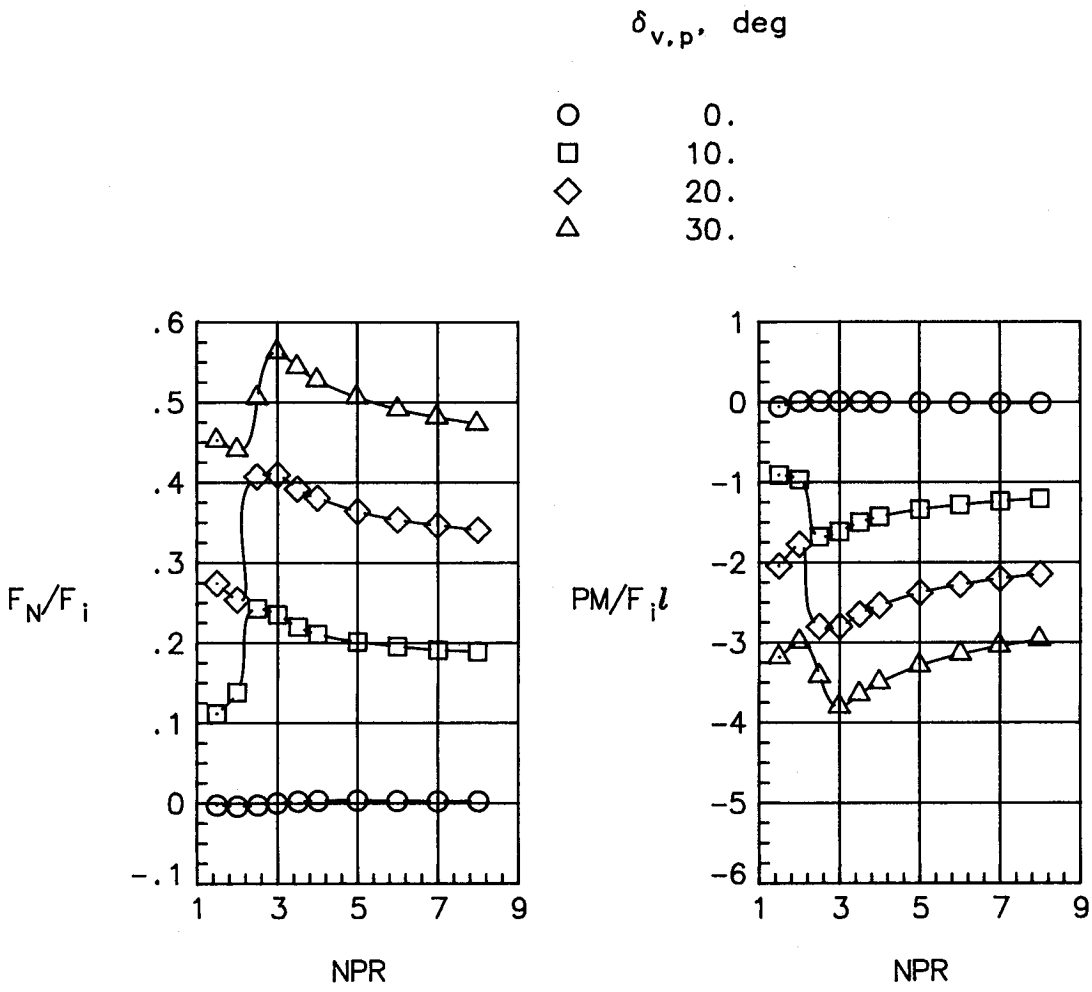

(b) Force and moment characteristics.

Figure 14. Concluded.

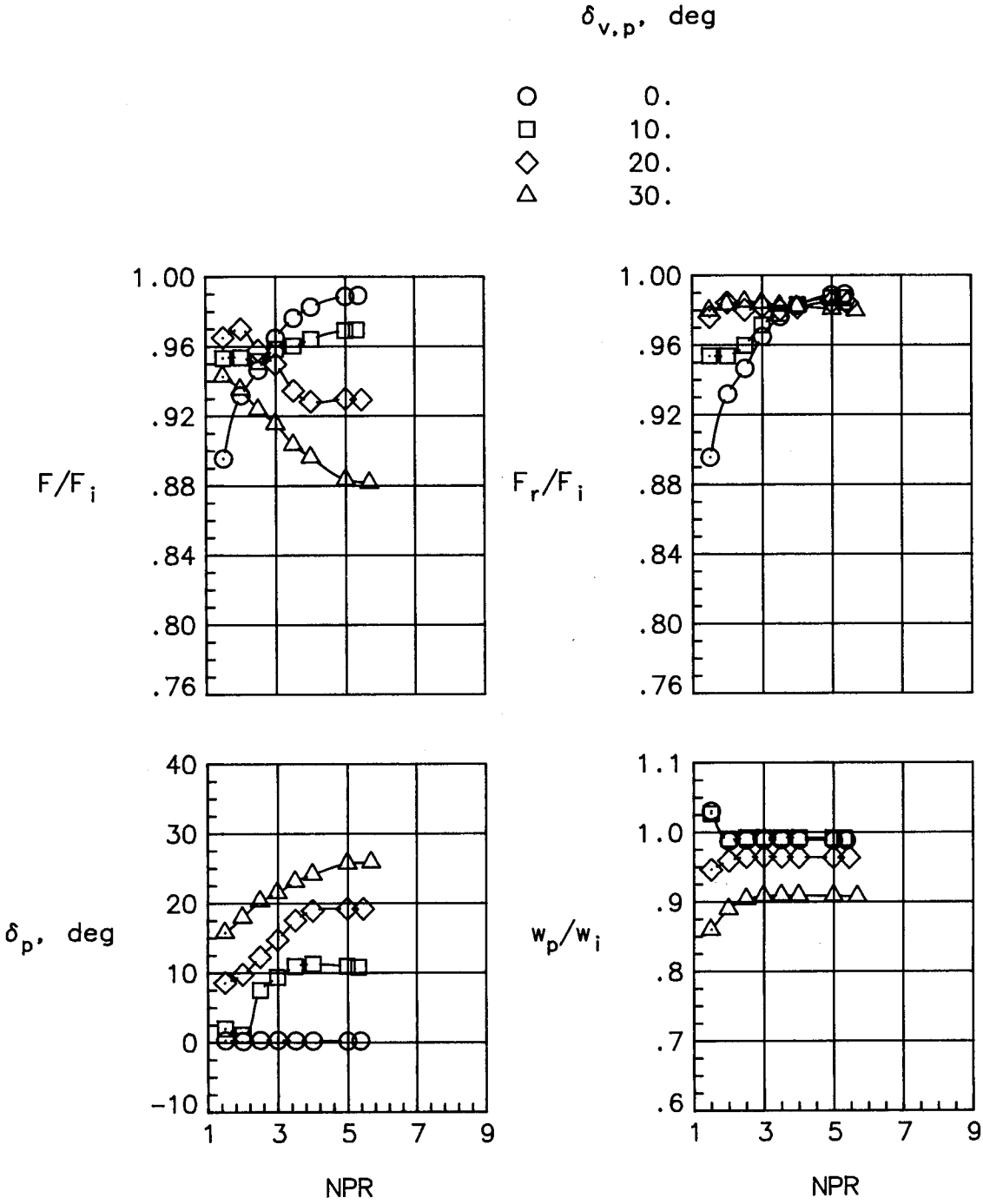

(a) Thrust and turning performance.

Figure 15. Effect of pitch vectoring on internal performance. A/B power; $L_f/d_t = 0.64$.

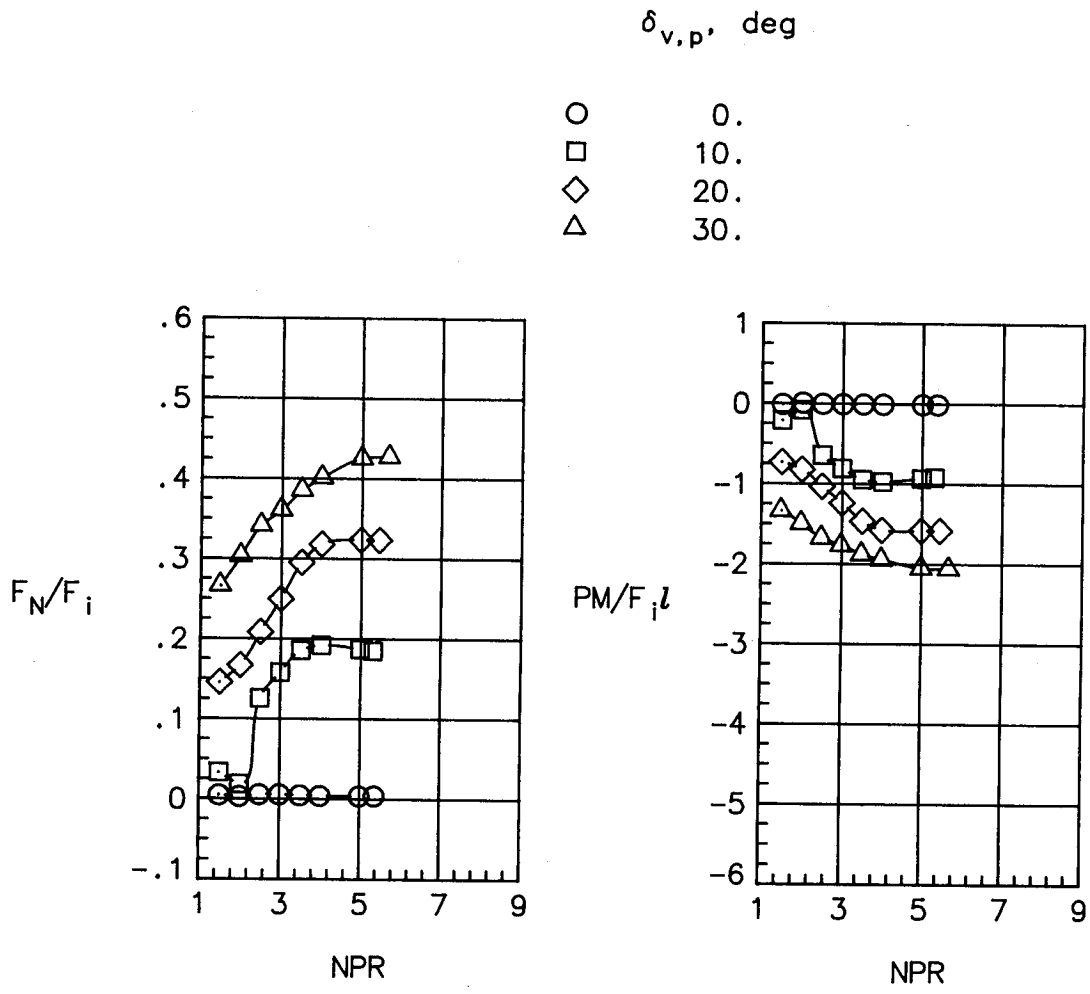

(b) Force and moment characteristics.

Figure 15. Concluded.

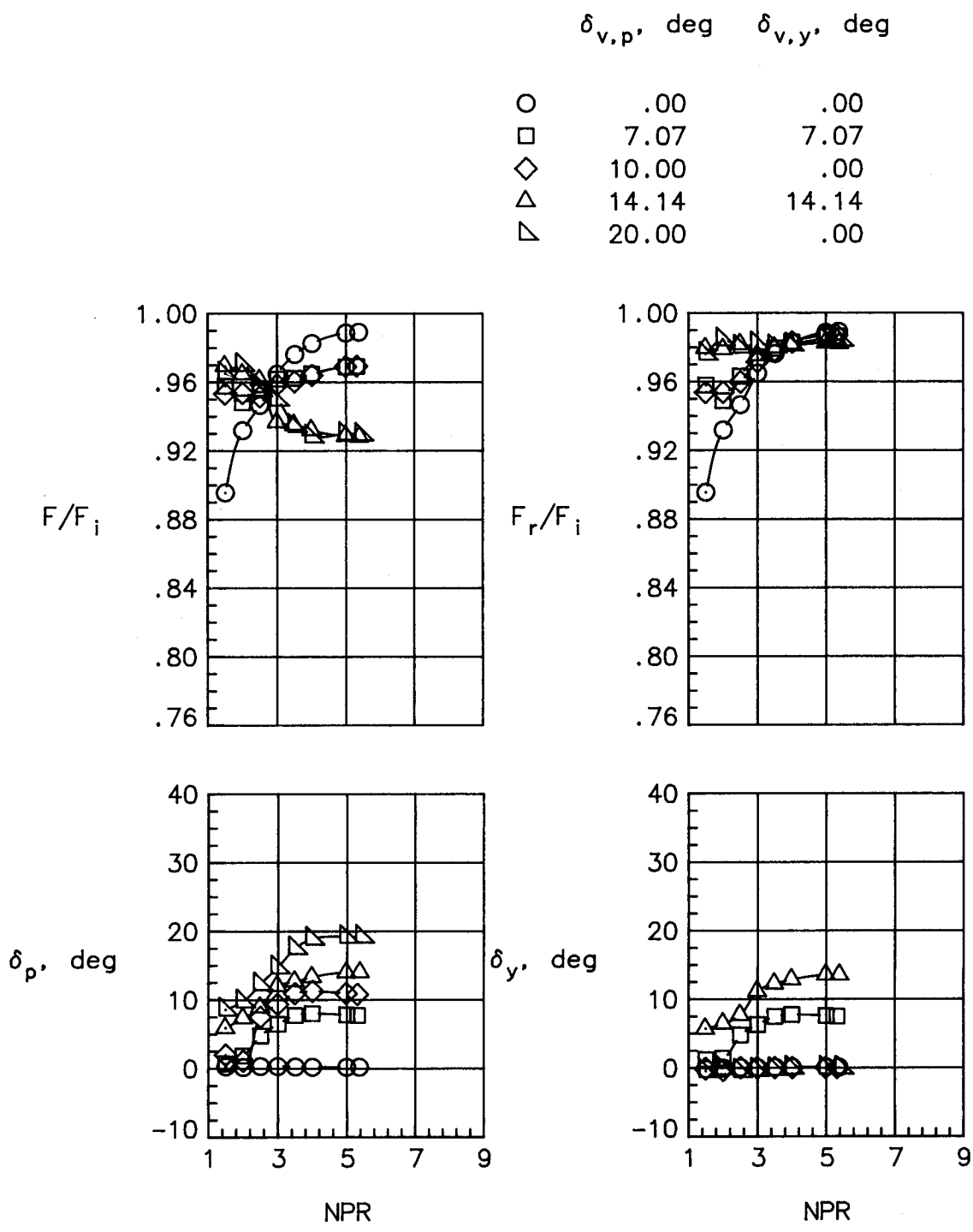

(a) Thrust and turning performance.

Figure 16. Effect of combined vectoring on internal performance. A/B power; $L_f/d_t = 0.64$.

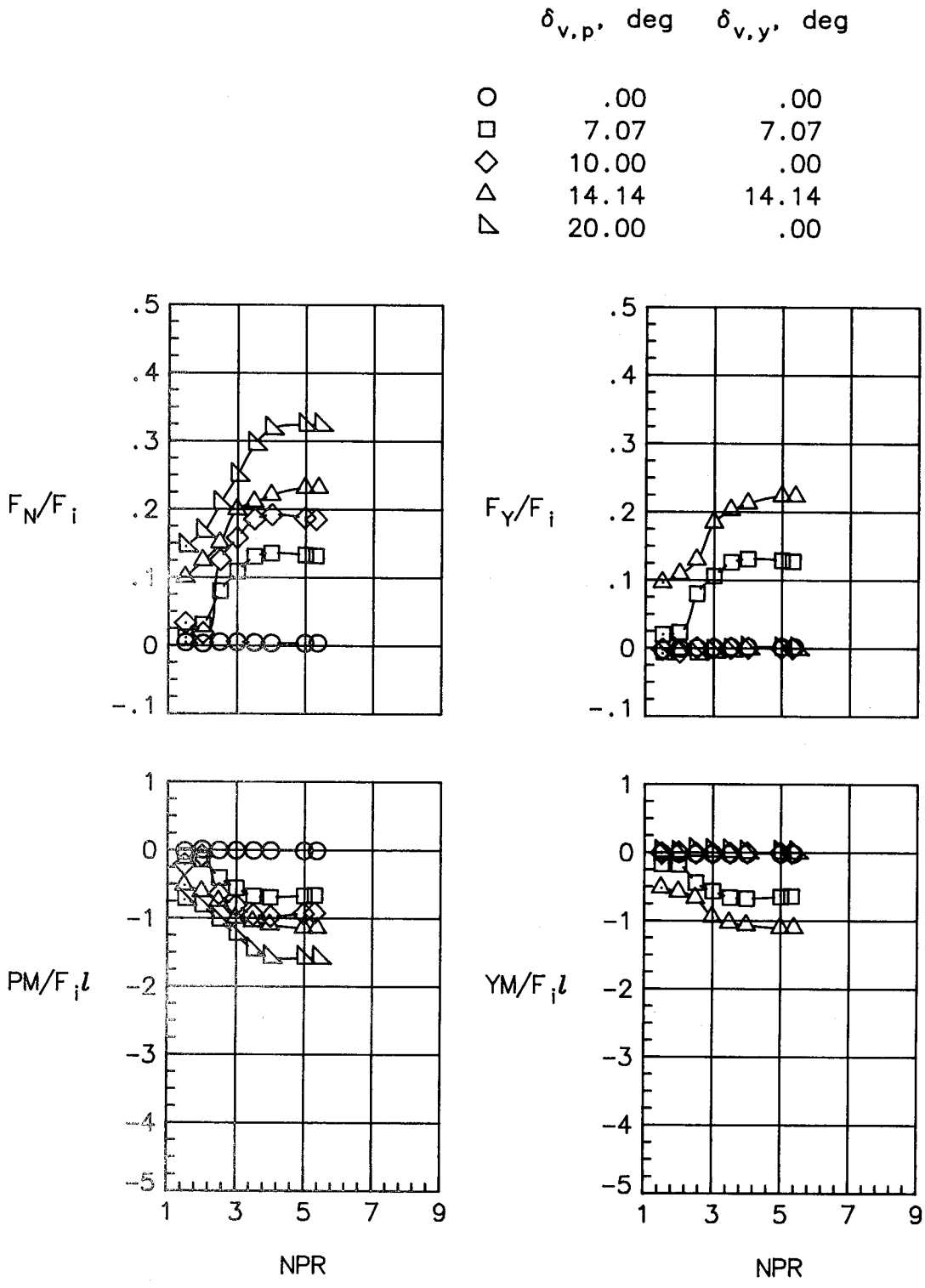

(b) Force and moment characteristics.

Figure 16. Concluded.

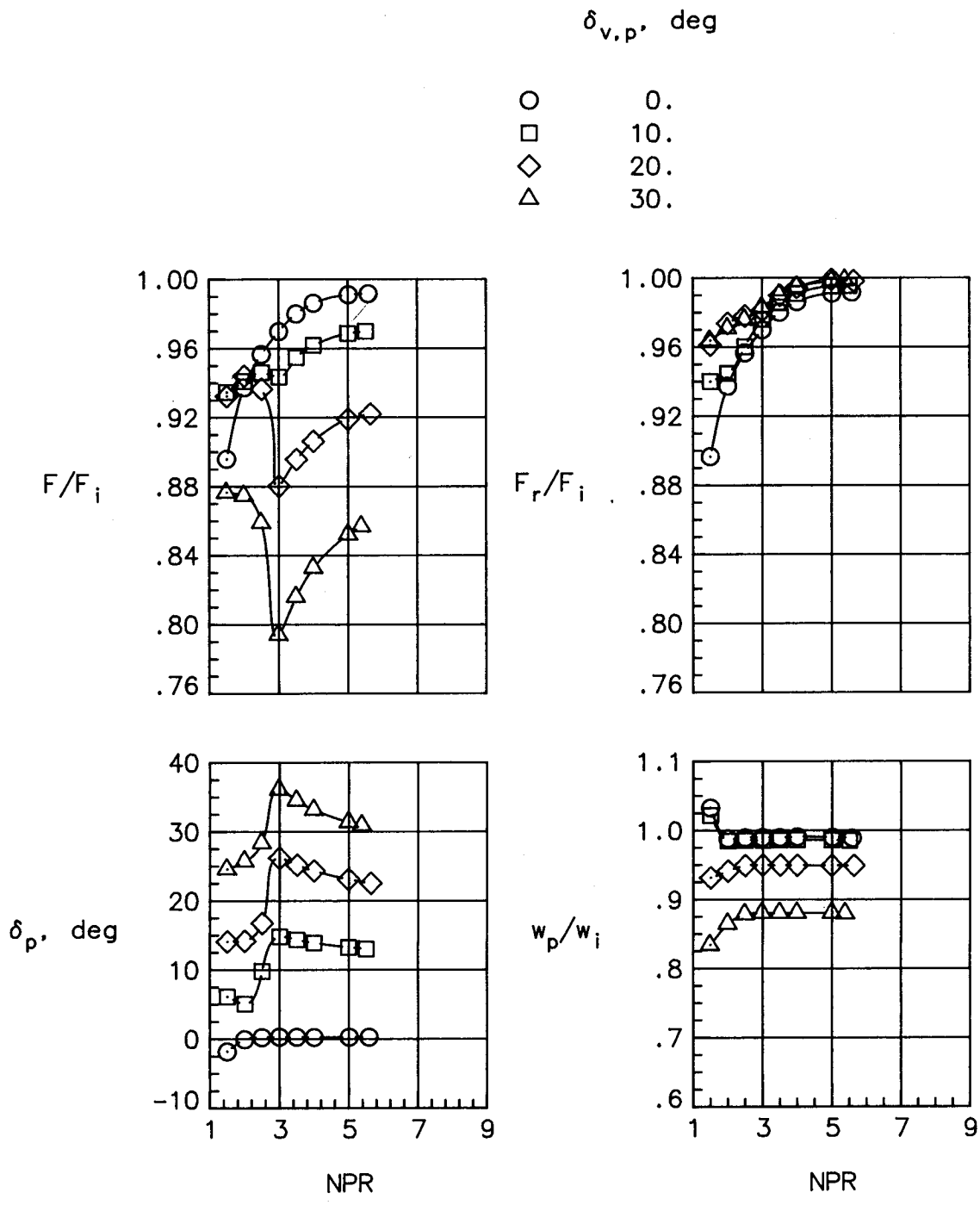

(a) Thrust and turning performance.

Figure 17. Effect of pitch vectoring on internal performance. A/B power; $L_f/d_t = 0.97$.

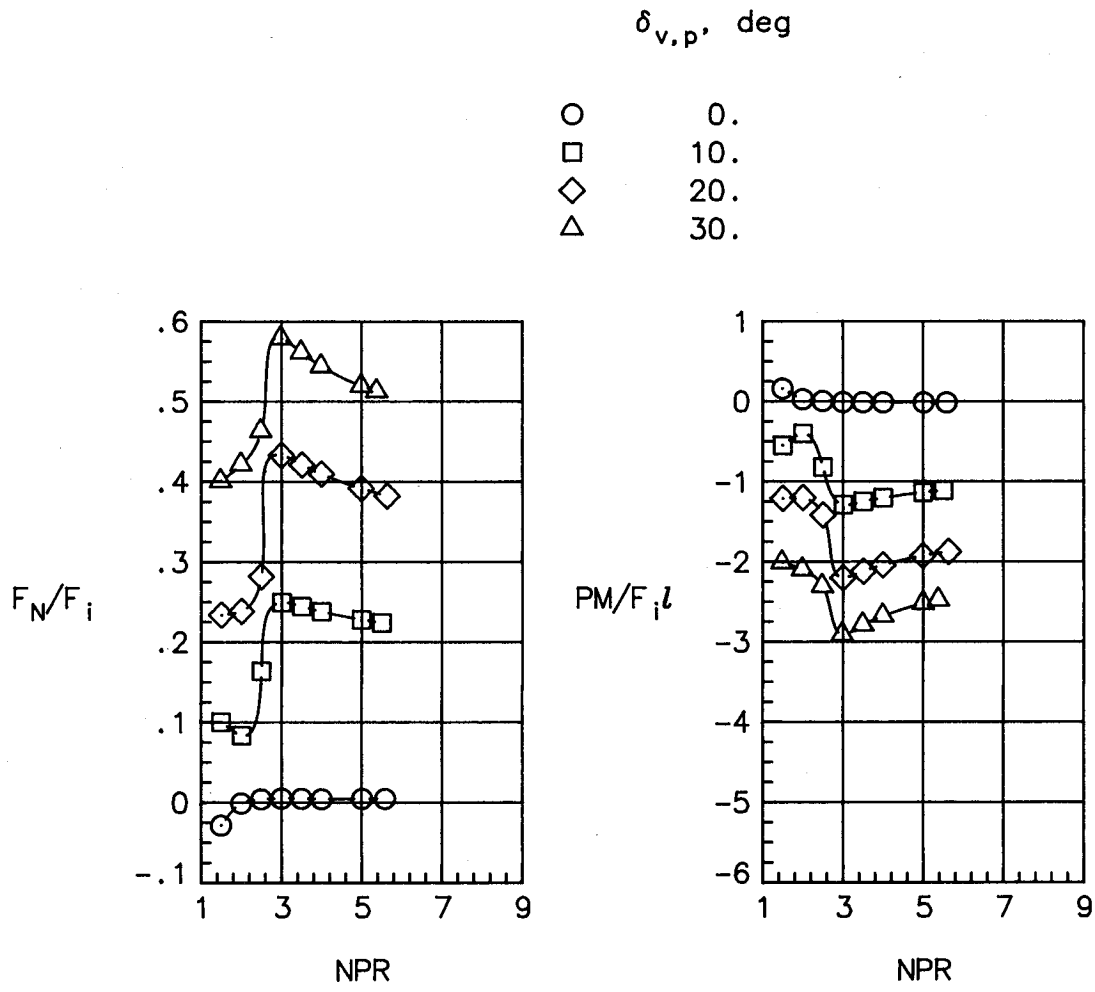

(b) Force and moment characteristics.

Figure 17. Concluded.

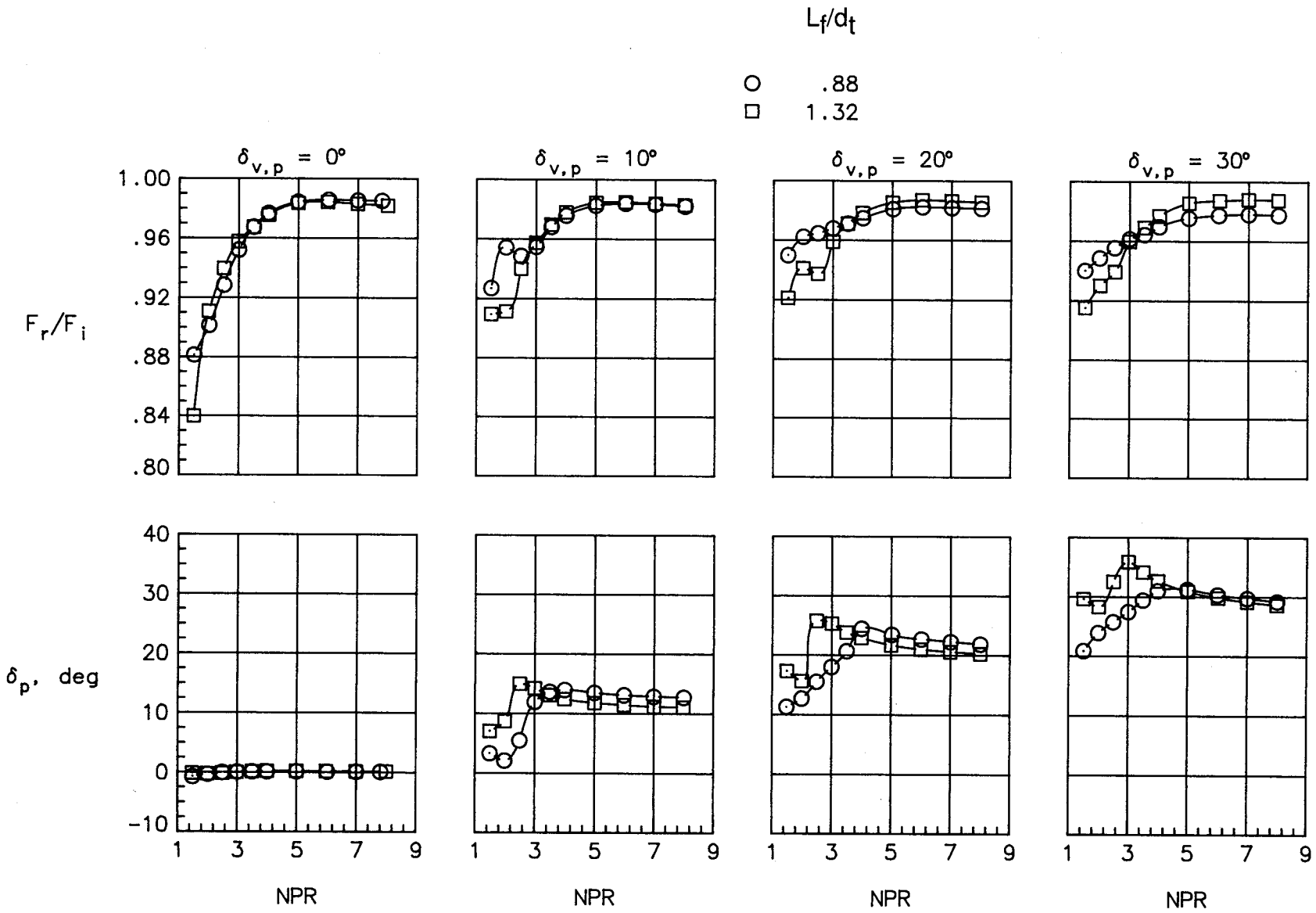

Figure 18. Effect of nozzle flap length on performance. Dry power.

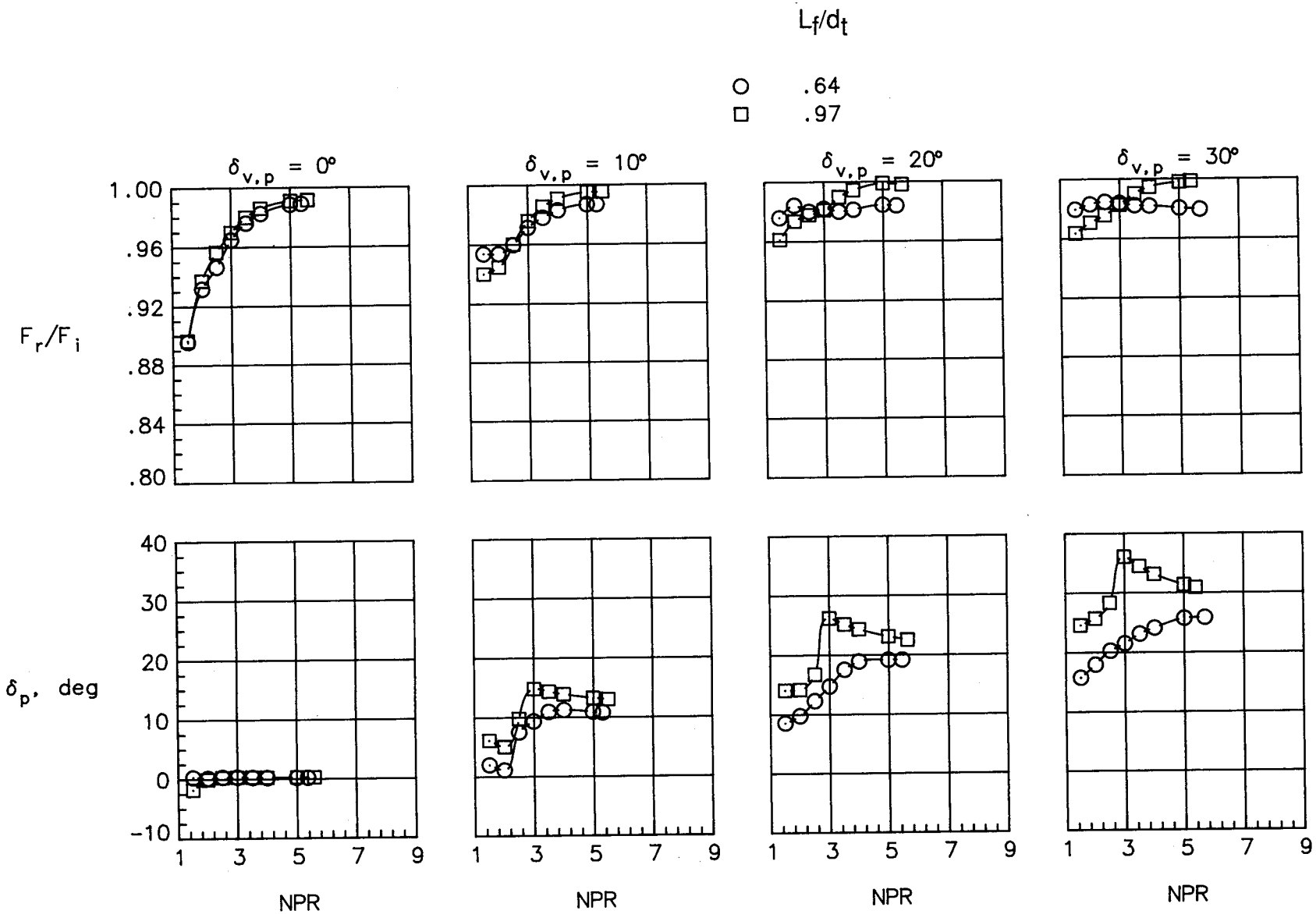

Figure 19. Effect of nozzle flap length on performance. A/B power.

NASA
National Aeronautics and Space Administration

Report Documentation Page

1. Report No.	2. Government Accession No.	3. Recipient's Catalog No.
NASA TM-4237		

4. Title and Subtitle	5. Report Date
Static Internal Performance of an Axisymmetric Nozzle With Multiaxis Thrust-Vectoring Capability	February 1991
	6. Performing Organization Code

7. Author(s)	8. Performing Organization Report No.
George T. Carson, Jr., and Francis J. Capone	L-16809

9. Performing Organization Name and Address	10. Work Unit No.
NASA Langley Research Center Hampton, VA 23665-5225	505-62-71-01
	11. Contract or Grant No.

12. Sponsoring Agency Name and Address	13. Type of Report and Period Covered
National Aeronautics and Space Administration Washington, DC 20546-0001	Technical Memorandum
	14. Sponsoring Agency Code

15. Supplementary Notes

16. Abstract

An investigation has been conducted in the static test facility of the Langley 16-Foot Transonic Tunnel to determine the internal performance characteristics of a multiaxis thrust-vectoring axisymmetric nozzle. Thrust vectoring for this nozzle was achieved by deflection of only the divergent section of the nozzle. The effects of nozzle power setting and divergent flap length were studied at nozzle deflection angles of 0° to 30° at nozzle pressure ratios up to 8.0.

17. Key Words (Suggested by Authors(s))	18. Distribution Statement
Axisymmetric nozzle Pitch vectoring Yaw vectoring Internal performance	Unclassified—Unlimited Subject Category 02

19. Security Classif. (of this report)	20. Security Classif. (of this page)	21. No. of Pages	22. Price
Unclassified	Unclassified	75	A04

For sale by the National Technical Information Service, Springfield, Virginia 22161-2171